Since January 2020 Elsevier has created a COVID-19 resource centre with free information in English and Mandarin on the novel coronavirus COVID-19. The COVID-19 resource centre is hosted on Elsevier Connect, the company's public news and information website.

Brain, Behavior, and Immunity 109 (2023) 251–268

Contents lists available at ScienceDirect

Brain Behavior and Immunity

journal homepage: www.elsevier.com/locate/ybrbi

Full-length Article

Blood-brain barrier penetration of non-replicating SARS-CoV-2 and S1 variants of concern induce neuroinflammation which is accentuated in a mouse model of Alzheimer's disease

Michelle A. Erickson [a,b], Aric F. Logsdon [a,b], Elizabeth M. Rhea [a,b], Kim M. Hansen [a], Sarah J Holden [c], William A Banks [a,b,*], Jessica L. Smith [d,e], Cody German [d,e], Susan A. Farr [f,g], John E. Morley [g], Riley R Weaver [a], Alec J. Hirsch [d,e], Andrej Kovac [h], Eva Kontsekova [h], Kristen K. Baumann [a], Mohamed A. Omer [a], Jacob Raber [c,i]

[a] Geriatrics Research Educational and Clinical Center, Veterans Affairs Puget Sound Health Care System, Seattle, WA, USA
[b] Division of Gerontology and Geriatric Medicine, Department of Medicine, School of Medicine, University of Washington, Seattle, WA, USA
[c] Department of Behavioral Neurosciences, Oregon Health and Science University, Portland, OR, USA
[d] The Vaccine and Gene Therapy Institute, Oregon Health and Sciences University, Beaverton, OR, USA
[e] Division of Pathobiology and Immunology Oregon National Primate Research Center, Oregon Health and Sciences University, Beaverton, OR, USA
[f] Saint Louis Veterans Affairs Medical Center, Research Service, St. Louis, MO, USA
[g] Division of Geriatric Medicine, Saint Louis University School of Medicine, St. Louis, MO, USA
[h] Institute of Neuroimmunology, Slovak Academy of Sciences, Bratislava, Slovak Republic
[i] Department of Neurology, Psychiatry, and Radiation Medicine, Division of Neuroscience, Departments of Neurology and Radiation Medicine, Oregon National Primate Research Center, Oregon Health Sciences University, Portland, OR, USA

ARTICLE INFO

Keywords:
COVID-19
SARS-CoV-2
Blood–brain barrier
Neuroinflammation
Alzheimer's disease
Obesity
Glycoprotein
Virus
Microglia
Aging

ABSTRACT

COVID-19 and especially Long COVID are associated with severe CNS symptoms and may place persons at risk to develop long-term cognitive impairments. Here, we show that two non-infective models of SARS-CoV-2 can cross the blood–brain barrier (BBB) and induce neuroinflammation, a major mechanism underpinning CNS and cognitive impairments, even in the absence of productive infection. The viral models cross the BBB by the mechanism of adsorptive transcytosis with the sugar *N*-acetylglucosamine being key. The delta and omicron variants cross the BB B faster than the other variants of concern, with peripheral tissue uptake rates also differing for the variants. Neuroinflammation induced by icv injection of S1 protein was greatly enhanced in young and especially in aged SAMP8 mice, a model of Alzheimer's disease, whereas sex and obesity had little effect.

1. Introduction

COVID-19, the acute respiratory illness induced by SARS-CoV-2, is followed in over 50 % of cases by Long COVID (Blomberg et al., 2021). Long COVID has many symptoms that are likely mediated by the CNS and has a very persistent course in which peripheral symptoms (e.g. fever, cough) tend to resolve while CNS symptoms (e.g., brain fog, memory, speech and language issues) worsen (Davis et al., 2021; Jones et al., 2021). COVID-19 and, in particular, Long COVID is associated with memory deficits and cognitive decline (Blomberg et al., 2021; Davis et al., 2021; Hampshire et al., 2021). CNS effects of COVID-19 include both neurological (Moghimi et al., 2021) and neuropsychiatric (Steardo et al., 2020) manifestations of post-acute sequelae of SARS-CoV-2 infection (PASC). For example, in those with severe symptoms of COVID-19, anxiety, attention, semantic word fluency and analogies, coronary heart disease, and pulmonary and lung function, and dizziness are more severe (Taquet et al., 2021; Widmann et al., 2021).

Several mechanisms can transform a virally-induced, acute respiratory infection into a long-term condition with predominant CNS symptomatology (Banks and Erickson, 2022; Xie et al., 2022). A common

* Corresponding author.
E-mail address: wabanks1@uw.edu (W.A. Banks).

https://doi.org/10.1016/j.bbi.2023.01.010
Received 11 July 2022; Received in revised form 19 December 2022; Accepted 16 January 2023
Available online 20 January 2023

pathway of those mechanisms and of conditions resulting in long-term cognitive impairments is neuroinflammation. One mechanism is by disruption of the blood–brain barrier (BBB) by cytokines, the ectodomain of the spike protein (S1), or SARS-CoV-2 (Buzhdygan et al., 2020; Kim et al., 2021; Nuovo et al., 2022; Zhang et al., 2021a). BBB disruption is an early biomarker in the development of cognitive impairments (Montagne et al., 2015; Montagne et al., 2020; Nation et al., 2019). Another mechanism by which neuroinflammation could be induced is by the cytokines released into blood during the cytokine storm of COVID-19 (Wang et al., 2020) crossing the BBB to enter brain. Another mechanism is by the ectodomain of the Spike protein (S1) itself or the intact virus crossing the blood–brain barrier (BBB). S1 has been shown to cross the BBB (Rhea et al., 2021) and staining has been detected in cortical neurons and along brain endothelial cells (Song et al., 2021) and viral interactions with the BBB can induce CNS changes (Stefano et al., 2022). SARS-CoV-2 can infect and cross in vitro models of the BBB (Krasemann et al., 2022; Yang et al., 2022), but it is not clear whether the virus can cross the in vivo intact BBB. Once in the brain, cytokines, S1, and virus can induce neuroinflammation (Frank et al., 2022; Theoharides, 2022) and cause cognitive impairments (Banks et al., 2001; Frank et al., 2022; Tangpong et al., 2006).

A concern raised in the literature is that Long COVID may worsen, accelerate, or unmask Alzheimer's disease (AD) and other neurodegenerative diseases or produce its own type of long-term cognitive impairment (Hascup and Hascup, 2020; Manzo et al., 2021; Meier et al., 2021; Miners et al., 2020; Silva et al., 2022). Risk factors for COVID-19 and Long COVID have similarities to those for AD. Risk factors for being infected and for having more severe COVID-19 include being male, obese, elderly, and having hypertension (Denson et al., 2021; Gebhard et al., 2020; Li et al., 2020; Zhang et al., 2020). Risk factors for acquiring Long COVID are being female, overweight, and between the ages of 45 and 65 (Jones et al., 2021; Pelà et al., 2022; Vanichkachorn et al., 2021; Vimercati et al., 2021). Infection rate, morbidity, including worsening cognition, and mortality from COVID-19 are increased in those with cognitive impairments, including AD (Tahira et al., 2021; Zhang et al., 2021b).

Transcriptomic and interactomic analyses indicate that the higher levels of amyloid beta peptide, which are associated with AD, play a part in the worsened outcomes for COVID-19 (Chiricosta et al., 2021). The effect of these risk factors has not been evaluated for their effects on neuroinflammation, likely a key risk factor for developing SARS-CoV-2-related cognitive impairments.

Here, we assess the relation of these risk factors to induce neuroinflammation. We show that a S-pseudotyped lentivirus (SARS-PV) and a virus-like particle (VLP) model of SARS-CoV-2 each cross the BBB even more rapidly than the S1 protein and that the viral models and S1 each induce neuroinflammation. Both SARS-PV and VLPs cross the BBB using the mechanism of adsorptive transcytosis with the sugar *N*-acetylglucosamine being key to transport and tissue uptakes. Variants of S1 differ in their uptake rates by brain and peripheral tissues. Neuroinflammation induced by icv injection of S1 protein was greatly enhanced in the SAMP8 AD mouse model, which develops with aging an amyloid precursor protein (APP)/amyloid beta peptide dependent cognitive impairment (Kumar et al., 2000; Morley et al., 2012). These results support that SARS-CoV-2 can cross the BBB and induce neuroinflammation, even in the absence of productive infection, particularly in the presence of an AD phenotype.

2. Methods

2.1. Synthesis of SARS-PV, VLPs, and null virus.

A plasmid expressing codon-optimized SARS-CoV2 spike protein with a C-terminal 21-aa ER retention signal deletion (SARS-CoV2-SpikeD21) was co-transfected with a GFP-expressing lentiviral vector (pGIPZ; Horizon Bioscience) and lentiviral packaging plasmid (pSPAX2; Addgene) into Expi293F suspension cells using the ExpiFectamine 293 transfection kit (Gibco) according to the manufacturer's instructions. At 6 days post-transfection, cells were pelleted by low speed centrifugation and supernatants were collected and filtered through a 0.45uM filter. Pseudoviruses were then pelleted by ultracentrifugation at 20,000xg for 2 h. Pellets were resuspended in PBS, aliquoted, and stored at −80C. Total particle numbers were determined by quantitative p24 ELISA and number of transducing particles quantitated on ACE2-expressing HEK293 cells. For the null (no S protein) virus, transfection was as above without the S encoding plasmid.

VLPs: Plasmid expression vectors encoding each of the SARS-CoV-2 M, E, N, and S proteins were constructed by standard cloning methods, using synthesized codon optimized sequences based on the WA-1 strain of SARS-CoV-2. Plasmids were transfected in combination into 200ml suspension-grown Expi293F cells based on previous work using Expifectamine reagent (ThermoFisher). 200 μg total plasmid DNA was transfected at a ratio of the 5:1:5:1 for the M:E:N:S plasmids. VLPs were collected from supernatant five days post transfection, passed through a 0.45 μm filter, and centrifuged 20 % sorbitol cushion at 30,000 rpm for 2 h in an SW32 rotor (Beckman). The pellet was then resuspended in 1/100th original volume of phosphate-buffered saline. The presence of viral proteins in the VLP pellet was confirmed by western blotting, using specific antibodies for viral proteins. Total protein content was assessed by BCA assay and VLPs were assessed by the OHSU Electron Microscopy Shared Resource to verify VLP structure. As a control, supernatant from mock transfected Expi293F cells was subjected to identical purification steps and resuspension.

2.2. Radioactive labeling of S1 (RayBiotech), SARS-PV, VLPs, and albumin

The S1 protein obtained from RayBiotech (230–30161, Val16-Fln690) was labeled with ^{125}I by the chloramine-T method (Montelaro and Rueckert, 1975) and purified on a column of G-10 Sephadex (I-S1). Bovine serum albumin (Sigma) was labeled with ^{99m}Tc by the stannous tartrate method (Wang et al., 2007) or with ^{131}I by the chloramine-T method and purified on a column of G-10 Sephadex (*T*-Alb; I-Alb). *T*-Alb and I-Alb were used interchangeably as per convenience. SARS-PV and VLPs were labeled by the Bolton-Hunter method (Perkin-Elmer) and purified on a column of Sepharose CL 2B (I-SARS-PV). Preliminary experiments found that the viruses are unstable if labeled by the chloramine-T method.

2.3. Brain perfusion: Brain uptakes of I-S1, I-SARS-PV, null virus, and VLPs.

Preliminary studies found that iv injected I-SARS-PV degraded too quickly to measure BBB permeability. Therefore, we used the brain perfusion method to study viral uptake. Brain perfusion has several characteristics that differentiate it from iv injection studies: it does not allow the virus to interact with blood-borne elements, it does not allow virus to interact with peripheral tissues prior to interaction with the BBB, and it does not involve recirculation of virus. As such, only direct interactions of virus with brain endothelial cells are assessed. Mice anesthetized to effect with 40 % urethane had the heart exposed via thoracotomy, the descending aorta clamped, and the jugulars cut bilaterally to prevent infused solution from recirculating. The left ventricle of the heart was cannulated and infused with Zlokovic's buffer (Zlokovic et al., 1986) at a rate of 2 ml/min. The perfusion contained 10^5 cpm/ml of the vascular marker I-Alb and $5x10^5$ cpm/ml of either I-S1, I-SARS-PV, iodinated null virus, or I-VLP. Mice were perfused for 2, 4, 6, 8, and 10 min, 2 mice at each time point, at which time mice were decapitated, the brain removed and weighed, and the levels of ^{125}I and ^{131}I determined in both brains and perfusion fluid. Brain/perfusion fluid ratios are calculated and the ratio for I-Alb subtracted from that for I-S1 or virus to yield the delta brain/perfusion ratio. As albumin subtracts

vascular content, this delta value reflects only virus taken up by the BBB. Removal of vascular space as a variable also reduces statistical variance for the viral ratio, improving statistical power in the subsequent calculations. The delta ratio was plotted against the perfusion time and the slope for the linear portion of this regression measures the unidirectional influx constant (Ki) in units of μl/g-min. The Ki was also determined for I-S1 using the brain perfusion method.

For determination of the effect of wheatgerm agglutinin (WGA) and brain regions on I-SARS-PV uptake by brain, a single time point of 5 min of brain perfusion was used. WGA was included in the perfusion solution at a concentration of 1 μg/ml.

2.4. Effect of lectins and sugars on brain and peripheral tissue uptakes of I-S1

One of six lectins was included at a dose of 10 μg/mouse in an injection into the right jugular vein of I-S1 and *T*-Alb. The lectins were WGA, Lycopersicon esculentum lectin (LEL), Lotus tetragonolobus lectin (LTL), Ricinus communis agglutinin (RCA), Galanthus nivalis lectin (GNL), and Sambucus nigra lectin (SNA). In other mice, one of four sugars at a dose of 100 μg/mouse was included in the injection of I-S1 and *T*-Alb into the right jugular vein. The sugars were *N*-acetylglucosamine, *N*-acetylgalactosamine, sialic acid, and mannose-6 phosphate. Ten min after the iv injection, blood was obtained from the left carotid artery, the brain harvested and liver, lung, kidney, and spleen collected. Tissue/serum ratios were computed for I-S1 and *T*-Alb with units of μl/g and the delta tissue/serum ratio calculated by subtracting the ratio for *T*-Alb from the ratio for S1. The sugars, WGA, and GNL were purchased from Sigma and the other 4 lectins were purchased from Vector Laboratories.

2.5. Brain and peripheral tissue uptakes of S1 variants:

The South African variant (Antibodies-online Cat #ABIN6963739), the UK variant (Reprokine Cat #RKNCOVS1B117), the Brazilian variant (Antibodies-online Cat #ABIN696442), the delta variant (Antibodies-online Cat # ABIN7013339) or the omicron variant (Reprokine RKNCOVS10) were labeled and purified as described above for S1 from RayBiotech. The I-S1 variant with T-Alb was injected into the right jugular vein and 1, 3, 5, 7.5, 10, 15, 30, 45, or 60 min later, carotid artery blood, whole brain, lung, liver, spleen, and kidney were collected. The delta tissue/serum ratios were calculated as outlined above and plotted against exposure time (Expt) using the equation:

$$\text{Expt} = \left[\int_0^t \text{Cp(t)dt}\right] \Big/ \text{Cp(t)}$$

where Cpt is the concentration of radioactivity in serum at time = t. The slope of the linear portion of this line defined the unidirectional influx constant Ki in units of μl/g-min and its Y intercept defined Vi in units of μl/g which consists of the vascular space and other components that are in rapid equilibrium with the circulation.

2.6. Effects of antibodies on S1 brain and peripheral tissue uptakes

Mice anesthetized with urethane received an injection via the jugular vein containing $6x10^5$ cpm I-S1 and $3x10^5$ cpm I-Alb. Mice had included in the injection antibodies directed against S1 [Proteintech 91349-PTG (neutralizing antibody, 8 μg/mouse) or R&D Systems MAB105403 (5 μg/mouse)] and Control mice received an injection human IgG (R&D Systems #1–001-A, 8 μg/mouse). Other mice with separate controls (receiving 10 μg/mouse of mouse IgG1, Abcam) received 10 μg/mouse of either AX290 or AX677 (Axon Covidax, Bratislava, Slovakia), which are blocking antibodies directed against the spike protein (Kovacech et al., 2022). Ten minutes after the iv injection, carotid artery blood was obtained, the mouse decapitated, and the whole brain, spleen, a kidney, and portions of the liver and lung were harvested and weighed. The % Inj/ml of I-S1 was calculated using the equation:

$$\%\text{Inj/ml} = 100(\text{cpm/ml of serum})/(\text{cpm injected}).$$

The tissue serum ratio of I-Alb was subtracted from the tissue/serum for I-S1 as above and expressed in units of μl/g-tissue. The percent of the injected dose of I-S1 taken up by a tissue that was not accounted for by the albumin space (that is, vascular space and leakage) was expressed in units of %Inj/g and calculated using the equation:

$$\%\text{Inj/g} = (\text{Corrected tissue/serum ratio})(\%\text{Inj/ml})/1000$$

2.7. ICV injection of SARS-PV: Neuroinflammation

Mice were anesthetized with 4 % isoflurane (0.5 l/min) induction and 2 % maintenance. Using sterile technique, the skull was exposed by a midline incision and skin retraction. Mice had a hole bored in the right skull + 1.0 mm lateral and −1.0 mm posterior to the bregma. A 1.0 μl Hamilton syringe was introduced to a depth of 3.0 mm through this hole and 1.0 μl of lactated Ringer's solution (n = 3), or 1.0 μl I-SARS-PV containing lactated Ringer's (n = 3), was injected into the lateral ventricle of the brain over 15 s. The syringe was then removed and the skin over the skull closed with wound clips. Mice recovered on a heating pad for 1 h and returned to their home cage for 96 h. Mice were then anesthetized with urethane (4 g/kg; 0.2 ml; ip) and perfused with 0.1 M PBS followed by 4 % paraformaldehyde (PFA) in 0.1 M PBS. Brains were extracted, post fixed for 24 h in 4 % PFA at 4 °C, cryopreserved in 30 % sucrose PBS solution, and frozen in optimal cutting temperature (OCT) compound on dry ice. Brains were stored at − 80 °C degrees until cryosectioning. Brains were acclimated overnight at −20 °C and then cut with a Leica CM1950 cryostat at 30 μm-thick serial sections and stored in 0.1 M phosphate buffered saline (PBS) + 0.02 % sodium azide at 4 °C as free-floating sections before processing for immunofluorescence. 30 μm-thick serial coronal sections underwent antigen retrieval in 10 mM trisodium citrate (pH 8.5) and heated at 90 °C for 20 m. Free-floating tissue sections were permeabilized for 30 min at room temperature (RT) in 0.1 M PBS + 0.2 % Triton X-100 and blocked for 2 h at 37 °C in 0.1 M PBS + 0.05 % Triton X-100 (PBST) + 5 % normal donkey serum (Jackson ImmunoResearch). Sections were incubated in PBST + 1 % donkey serum overnight at 4 °C with the following antibodies: Green fluorescent protein (GFP, Goat, R&D Systems: AF4240, 1:100), Ionized calcium binding adaptor molecule 1 (Iba1, Rabbit, WAKO: 019–19741, 1:1,000), and Glial fibrillary acidic protein (GFAP, Chicken, Millipore: AB5541, 1:2,000). The following day, sections were washed and incubated for 2 h at RT in a 1:1,000 dilution of Alexa-fluor-conjugated secondary antibodies in PBST + 1 % donkey serum. Sections were then counterstained for DAPI, mounted, and cover slipped using Fluoromount-G (ThermoFisher, 4958–02). Imaging was conducted with a 10X objective on a Zeiss Axio Observer 7 inverted microscope.

To determine which cells took up SARS-PV, RNAScope was employed. Mouse 15 μm-thick coronal sections were mounted on microscope slides. In situ hybridization for mouse CCL5 mRNA was performed by RNAScope using protocols and reagents from the manufacturer (ACD, RNAScope Multiplex Fluorescent Reagent Kit v2). Briefly, dehydrated, peroxidase- and protease-blocked sections were hybridized with probes for the chosen cytokine, such a MmCCL5probe (ACD, 469601), for 2 h at 40 °C. The cytokine signal was developed by incubation with HRP-C1 probe for 15 m at 40 °C, followed by Opal570 substrate (Akoya Biosciences FP1488001KT, 1:1500 in ACD Amplification Buffer) for 30 min at 40 °C. Non-specific epitopes were blocked with Antibody Diluent/Block (Akoya ARD1001EA). To determine the cellular source of cytokine production, slides were incubated with anti-GFAP (Mouse, Covance: SMI-22R, 1:1000), anti-Iba1 (Rabbit, WAKO: 019–19741, 1:1000), anti-NEUN (Rabbit, Abcam: ab10422F5, 1:1000), or GLUT1 (Rabbit: Millipore: 07–1401, 1:1000) and incubated with Opal polymer HRP secondary antibody (Akoya ARH1001EA). Slides were

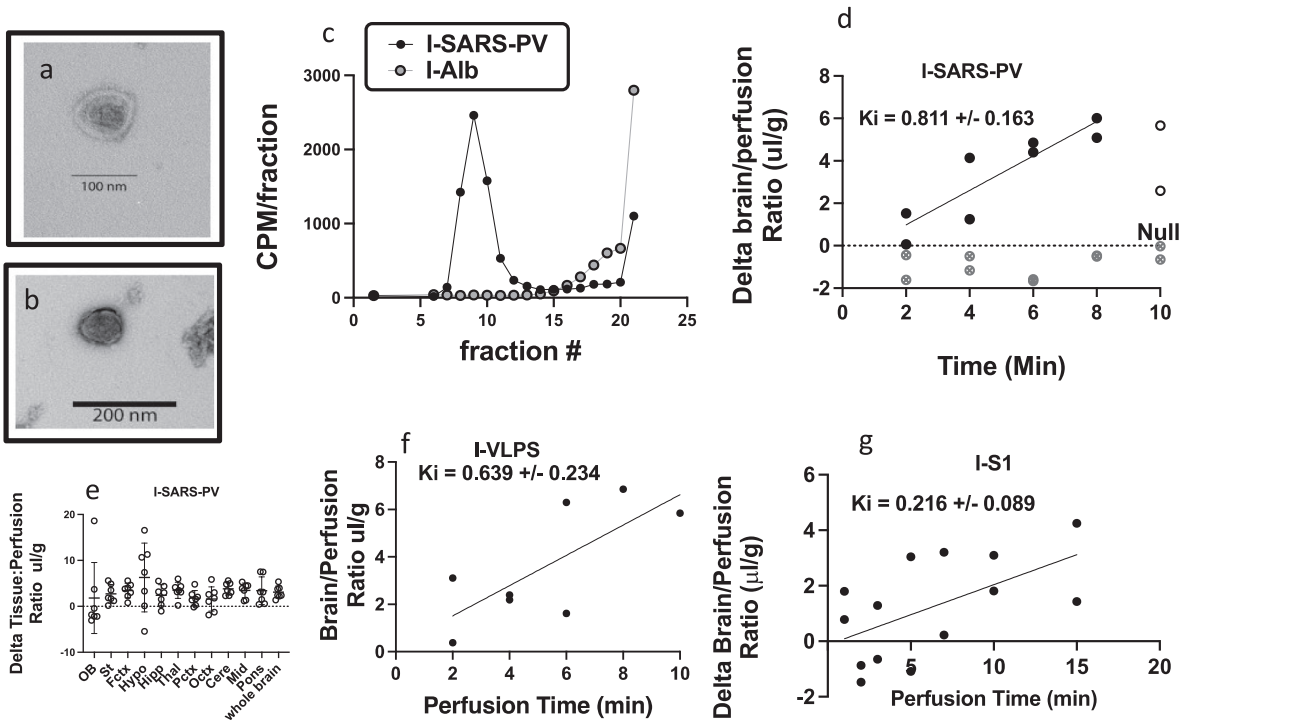

Fig. 1. Blood-brain barrier transport of SARS-PV, VLP, null virus, and S1. Panels a & b show electron micrographs of SARS-PV. Panel c shows elution patterns of radioactively labeled SARS-PV and albumin from a column of Sepharose CL 2B. Panel d shows the transport of I-SARS-PV across the BBB with a Ki = 0.811 ± 0.163 µl/g-min and a Vi = (−) 0.641 ± 0.891 µl/g (r^2 = 0.805, n = 8, p = 0.0025). Panel d also shows null virus which did not cross the BBB. The open circles departed from linearity and so were not included in the calculation of Ki. Panel e shows that the uptake of I-SARS-PV across brain regions was homogeneous. Panel f shows the transport of I-VLPs across the BBB with a Ki = 0.639 ± 0.234 µl/g-min and a Vi = 0.234 ± 1.4 µl/g (r^2 = 0.555, n = 8, p = 0.034). Panel g shows for comparison I-S1, which had a Ki = 0.216, which was similar to that previously reported, but much lower than the transport rates for SARS-PV or VLPs.

developed with Opal520 substrate (Akoya FP1487001KT, 1:100 in 1x Plus Amplification Diluent, Akoya FP1498) for 10 m at RT. Slides were counterstained with DAPI, coverslips mounted, and imaged as above.

2.8. Effects of IP or ICV S1 on cytokines, amyloid, and metabolic hormone levels

Young (2 mo old) CD-1 male mice received an IP injection with or without 10 µg/mouse of S1 protein (AMSBIO); these mice had been anesthetized with isoflurane prior to the IP injection to match the icv injection groups below. 24 h later, whole blood was collected from the abdominal aorta and the brain perfused with cold lactated Ringer's solution to wash out its vascular space. Hemi-brains were frozen in liquid nitrogen until homogenized with an Omni beadbeater in phosphate buffered solution containing 0.1 % triton and phosphatase and protease inhibitor cocktails (Sigma P5726 and P8340), and centrifuged. The supernatant had its protein content determined by BCA and was analyzed for interleukin (IL)-1 alpha, IL-1 beta, IL-2, −3, −4, −5, −6, −9, −10, −12(p40), −12(p70), −13, −17, eotaxin, G-CSF, GM-CSF, INF-gamma, KC, MCP-1, MIP-1 alpha, MIP-1 beta, RANTES, and TNF (Bio-Plex Pro Mouse Cytokine 23-plex Assay, Bio-Rad). The blood collected from the abdominal aorta was allowed to clot and the resulting serum assayed in the 23 analyte bioplex.

Three sets of mice received an icv injection of S1 protein (AMSBIO) with brains being harvested 24 h later for the measurement of cytokines in the 23 analyte bioplex assay. In each set, mice were anesthetized with isoflurane and received an icv injection of 1 µl of lactated Ringer's solution with or without S1. The first set of mice was young (2 mo old) CD-1 male mice and received an injection of 0, 0.01, 0.1 or 1.0 µg/mouse of S1. The second set of mice was male or female CD-1 aged 2–4 mo or 16–18 mo of age and received 1.0 µg/mouse of S1. The third set of mice were male SAMP8 male aged 2 mo or 12 mo and received 1.0 µg/mouse of S1. Some of the 12 mo old SAMP8 male mice had been on a high fat diet (Research Diets, D12492i) since age 2 months. 24 h after the icv injection, brains were frozen in liquid nitrogen and blood was collected as above. Brains were homogenized with an Omni beadbeater in phosphate buffered solution containing 0.1 % Triton and phosphatase and protease inhibitor cocktails (Sigma P5726 and P8340), and centrifuged. The protein content of the supernatant was determined by BCA. Brain lysates were evaluated with the 23 bioplex, and serum levels of leptin, ghrelin, insulin, PAI-1, and resistin measured (Bio-Plex Pro Mouse Diabetes 8-plex Assay, Bio-Rad). Amyloid beta peptide 1–40 and amyloid beta peptide 1–42 were measured in the brain supernatants with the *Meso* K15199 rat/human Abeta kit. Body weights prior to the icv injection of S1 was also taken.

2.9. Brain and peripheral tissue uptake of S1 in young and aged SAMP8 mice

Male SAMP8 mice aged 4 or 12 months were anesthetized with urethane and given an injection into the jugular vein of 0.2 ml of lactated Ringer's solution containing $8x10^5$ cpm of I-S1 and $5X10^5$ cpm I-Alb. At 1–10 min after the iv injection, carotid artery blood was obtained, the mice decapitated, and brain, spleen, a kidney, and portions of the liver and the lung were removed and weighed. Radioactive levels were measured in a gamma counter and the tissue/serum ratios calculated for both I-S1 and I-Alb. The I-Alb tissue/serum ratio for each sample was subtracted from its I-S1 tissue/serum ratio, yielding the amount of I-S1 taken up by a tissue beyond that attributable to vascular space or leakage. These corrected tissue/serum ratios were plotted against time and compared for an effect of age and compared to historical data published for young CD-1 male mice (Rhea et al., 2021).

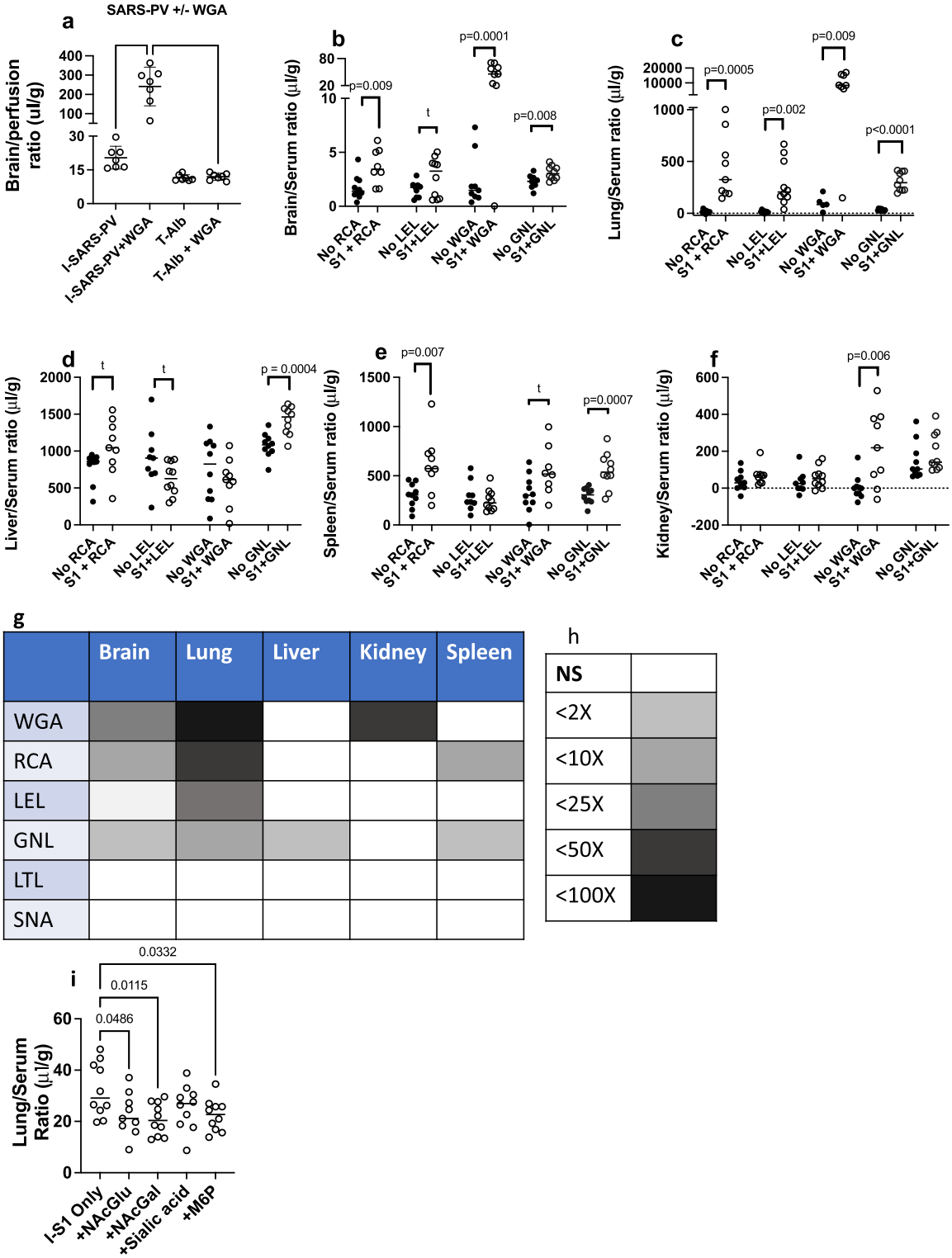

Fig. 2. Effects of lectins on SARS-PV and S1 uptake by brain and peripheral tissues. **a**, WGA increased SARS-PV brain uptake by over 10-fold [20.4 ± 1.9 µl/g to 241 ± 38 µl/g (df = 12, t = 8.05, p < 0.0001)] without disrupting the BBB to albumin. **b**, for brain, a significant increase in S1 uptake was induced by RCA (t = 2.97, df = 16, p = 0.009, n for control = 10, n for lectin = 8), WGA (t = 5.02, df = 17, p = 0.0001, n for control = 10, n for lectin = 9), and GNL (t = 2.96, df = 18, p = 0.008, n for control = 10, n for lectin = 10). **c**, for lung, a significant increase in S1 uptake was induced by RCA (t = 4.32, df = 17, p = 0.0005, n for control n = 10, n for lectin n = 9), LEL (t = 3.76, df = 17, p = 0.0016, n for control = 9, n for lectin = 10), WGA (t = 4.08, df = 12, p = 0.0015, n for control = 6, n for lectin = 8), and GNL (t =

9.71, df = 18, p < 0.0001, n for control = 10, n for lectin = 10). **d**, for liver, a significant increase is S1 uptake was induced by GNL (t = 4.33, df = 18, p = 0.0004, n for control n = 10, n for lectin n = 10). **e**, for spleen, a significant increase in S1 uptake was induced by RCA (t = 3.10, df = 17, p = 0.007, n for control n = 10, n for lectin n = 9) and GNL (t = 4.06, df = 18, p = 0.0007, n for control n = 10, n for lectin n = 10). **f**, for kidney, a significant increase in S1 uptake was induced WGA (t = 3.15, df = 17, p = 0.006, n for control = 10, n for lectin = 9). **g**, heat map of changes induced by lectins in the various tissues, LTL and SNA did not affect S1 uptake by any tissue. **h**, key to heat map showing fold increases for statistically significant changes (NS = not significant), **i**, shows sugar inhibition of I-S1 uptake by lung (n = 10/cell).

2.10. Statistics

Means of two groups were compared by *t*-test, whereas more than two groups was compared by ANOVA and the post-test for multiple comparisons was Newman-Keuls. Regression analysis was performed using the statistical package in Prism 9.0 (GraphPad, Inc, San Diego, CA) and slopes of linearities are reported with their error terms, r^2, n, and p values. Means are given with their standard deviations.

3. Results

3.1. SARS-PV and VLP, but not null virus, cross the BBB

Fig. 1a&b are electron microscopy of the SARS-CoV-2 VLP and Fig. 1c shows results for the purification of I-SARS-PV. The ability of I-SARS-PV, I-VLP, and I-S1 to cross the BBB were compared by perfusing the radiolabeled material through the vasculature of the brain, thus eliminating potential interactions with circulating substances and uptake or degradation by peripheral tissues. Passage of I-SARS-PV during brain perfusion was linear for about the first 8 min of perfusion (Fig. 1d) with a Ki = 0.811 ± 0.163 μl/g-min. Null virus did not show brain uptake and had brain/perfusion ratios less than those for smaller, co-perfused *T*-Alb (Fig. 1d). Perfused I-VLPs had an uptake rate similar to that of I-SARS-PV (Fig. 1f), but perfused I-S1 (Fig. 1g) had a lower uptake rate (0.215 ± 0.089 μl/g-min) than either of the two viral models, but similar to that previously published for iv administered I-S1 (Rhea et al., 2021). These results show that both virus models cross the BBB, that such crossing is dependent on the S protein, and that the viral particles cross the BBB more rapidly than S1.

3.2. All regions of brain take up SARS-PV

Uptake by various brain regions was determined by perfusing I-SARS-PV and *T*-Alb for 5 min and harvesting brains. Uptake by brain regions of I-SARS-PV administered by brain perfusion showed the lowest uptake for occipital cortex (1.6 μl/g) and the highest for hypothalamus (6.3 μl/g). ANOVA using repeated measures across brain regions showed no statistical differences and Newman-Keuls multiple comparisons test found no difference among the brain regions (Fig. 1e). Similar homogeneous uptake across brain regions was found for perfused I-VLP and I-S1.

3.3. Lectins affect tissue uptakes of I-SARS-PV and I-S1

Viruses most commonly use their attachment glycoproteins to bind to cell surface glycoproteins or glycolipids, inducing adsorptive endocytosis to enter cells (Marsh, 1984). We previously showed that the lectin WGA greatly increased uptake of S1 by brain and peripheral tissues (Rhea et al., 2021). Here, we determined whether SARS-PV uptake was also;ll mediated by the adsorptive transcytosis process. WGA was added to the brain perfusion fluid containing I-SARS-PV and Tc-Alb. WGA increased I-SARS-PV uptake by brain, but had no effect on Tc-Alb uptake (Fig. 2a). This demonstrates that SARS-PV as predicted by prior work with S1 is dependent on glycoprotein interactions for BBB penetration and that WGA does not increase SARS-PV uptake by disrupting the BBB.

The sugars most often associated with glycoprotein uptake of viruses are sialic acid, *N*-acetylglucosamine, *N*-acetylgalactosamine, mannose, and fucose (Shilatifard et al., 1993; Ushijima et al., 1992), with evidence that sialic acid and *N*-acetylglucosamine are involved in S1 binding and SARS-CoV-2 uptake (Baysal et al., 2021; Nguyen et al., 2022). Here we used lectins selective for these sugars (WGA: sialic acid and *N*-acetyl-D-glucosamine, LEL: *N*-acetylglucosamine and *N*-acetylgalactosamine, LTL: fucose arabinose, RCA: *N*-acetylgalactosamine and *N*-acetylglucosamine, GNL: mannose, SNA: sialic acid) to determine which were most likely to be involved in I-S1 transport across the BBB and uptake by peripheral tissues (Table 1). Brain, liver, spleen, kidney, and lung were harvested from each group of animals that received a single lectin. Each tissue was compared after lectin injection to its non-lectin injected control by *t*-test. Two lectins, LTL and SNA had no effect on I-S1 uptake for any tissue, indicating that fucose and sialic acid played little or no role in S1 binding (Fig. 2g). Brain uptake was robustly increased by WGA with lesser increases by RCA and by GNL, indicating an important role for *N*-acetylglucosamine, and perhaps minor ones for mannose and *N*-acetylgalactosamine. Lung had robust increases for WGA, RCA, LEL and GNL, indicating importance of *N*-acetylglucosamine, *N*-acetylgalactosamine and mannose. Only GNL increased uptake of I-S1 by liver (Fig. 2d). Spleen had increases for RCA and GNL, indicating the importance of *N*-acetylgalactosamine and mannose (Fig. 2e). Kidney had an increase only with WGA, indicating the importance of *N*-acetylglucosamine (Fig. 2f). The heat map and its key (Fig. 2g-h) shows

Table 1
Effects of lectins on tissue uptakes of I-S1. Results show percentage of control values.

	Tissue				
Lectin	Brain	Lung	Liver	Spleen	Kidney
WGA	1082***	11843**	78^{NS}	152^{NS}	5000**
LTL	134^{NS}	174^{NS}	73^{NS}	119^{NS}	43^{NS}
SNA	79^{NS}	116^{NS}	97^{NS}	115^{NS}	45^{NS}
RCA	211**	2684***	133^{t}	205**	187^{NS}
GNL	135*	949***	132***	186***	132^{NS}
LEL	174^{t}	1817**	69^{t}	86^{NS}	175^{NS}

NS = no significant change; 0.1 > t ≥ 0.05; *p < 0.05; **p < 0.01; ***p < 0.001.

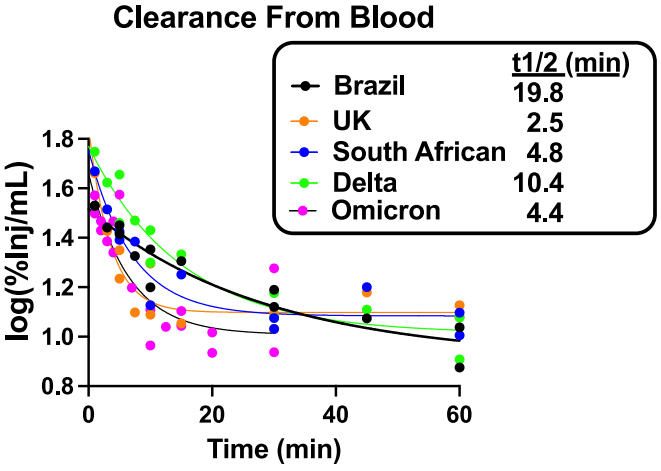

Fig. 3. Clearance of intravenously administered S1 variants from blood. The log values of %Inj/ml were plotted against time using a one phase decay model. Half life values were 2.45 min for the UK variant, 4.04 min for the Omicron variant, 4.85 min for the South African variant, 10.4 min for the Delta variant, and 19.8 min for the Brazilian variant.

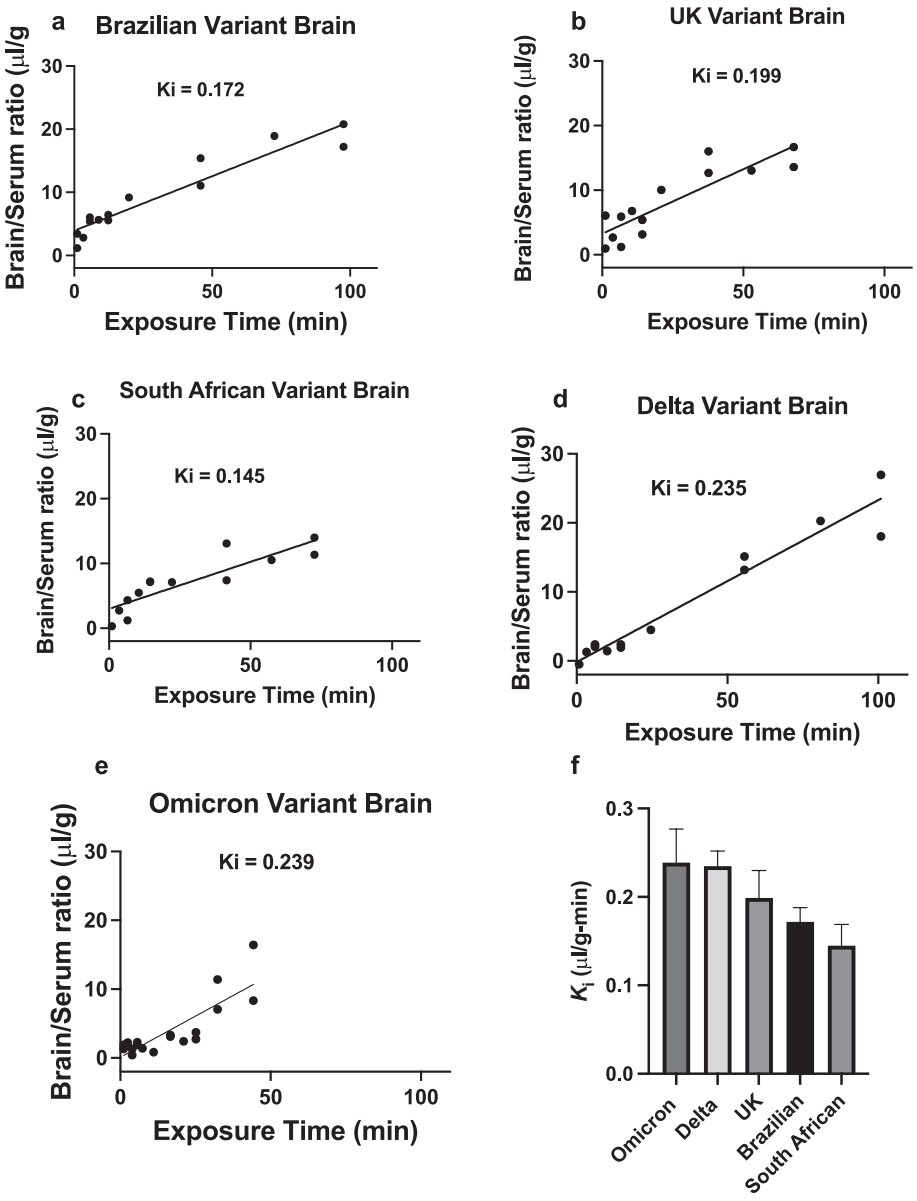

Fig. 4. Unidirectional influx constant (Ki) for blood-to-brain transport of S1 variants. **a**, for the Brazilian variant, the relation between brain/serum ratios and time was statistically significant ($r^2 = 0.907$, $n = 14$, $p < 0.0001$) and the Ki was 0.172 ± 0.016 µl/g-min, **b**, for the UK variant, the relation between brain/serum ratios and time was statistically significant ($r^2 = 0.772$, $n = 14$, $p < 0.0001$) and the Ki was 0.199 ± 0.031 µl/g-min, **c**, for the South African variant, the relation between brain/serum ratios and time was statistically significant ($r^2 = 0.769$, $n = 13$, $p < 0.0001$) and the Ki was 0.145 ± 0.024 µl/g-min, **d**, for the Delta variant, the relation between brain/serum ratios and time was statistically significant ($r^2 = 0.944$, $n = 13$, $p < 0.0001$) and the Ki was 0.235 ± 0.017 µl/g-min, **e**, for the Omicron variant, the relation between brain/serum ratios and time was statistically significant ($r^2 = 0.702$, $n = 19$, $p < 0.0001$) and the Ki was 0.239 ± 0.038 µl/g-min, **f**, shows comparison of Ki's for brain.

similarities between lung and brain in the effects of lectins on I-S1 uptake and a diversity of effects for other tissues. For lung, inclusion of the sugars *N*-acetylglucosamine, *N*-acetylgalactosamine, or mannose-6 phosphate, but not sialic acid, inhibited uptake of I-S1 (Fig. 2i). Only *N*-acetylgalactosamine inhibited uptake I-S1 uptake by liver ($p = 0.022$), although it produced a trend for brain ($p = 0.07$). The sugars had no effect on I-S1 uptake by kidney or spleen. These results indicate the importance of glycoproteins in the uptake of S1 by brain and peripheral tissues, but more strikingly, suggest a diversity in the cell surface binding sites used by S1.

3.4. Brain and peripheral tissue uptakes vary among the S1 variants

Several variants of SARS-CoV-2 have arisen that have variants in the S protein designated as the United Kingdom (UK, alpha, B.1.1.7), South African (beta, B.1.351), Brazilian (gamma, P.1), delta (B.1.617.2), and omicron (B.1.1.529) variants. These variants have different patterns of infectivity and severity of symptoms and so we determined and compared their rates of clearance from blood, BBB penetration, and uptake by peripheral tissues. Clearance from blood after iv injection was biphasic for all S1 variants with half-time clearances of the initial phase ranging from 2.5 min for the UK variant to 19.8 min for the Brazilian variant (Fig. 3). The unidirectional influx constant for blood-to-brain permeation varied from a low of 0.145 µl/g-min for the South African variant to 0.239 µl/g-min for omicron variant (Fig. 4). Peripheral tissues showed variation in their uptakes of the variants (Fig. 5). Any uptake rate greater than 3.9 µl/g-min showed nonlinear uptake consistent with reaching equilibrium. Most uptake rates greater than 20 µl/g-min showed a phase of decline after the initial uptake, consistent with release of S1 from the tissue back into the blood stream. The highest uptake rates for the Brazilian variant and the delta variant was by spleen (Fig. 5p,s) and the UK, South African, and omicron variants were most avidly taken up by liver (Fig. 5g,h,j). The variant most avidly taken up by lung was the UK variant (Fig. 5b), the liver took up the omicron variant most avidly (Fig. 5j), the kidney took up the UK variant more than any other variant (Fig. 5l), and the spleen took up the delta variant more rapidly than any other variant (Fig. 5s).

3.5. Antibodies against S protein can block brain uptake and alter uptake by other tissues and clearance from blood

Immunity is conferred after vaccination and natural infection by

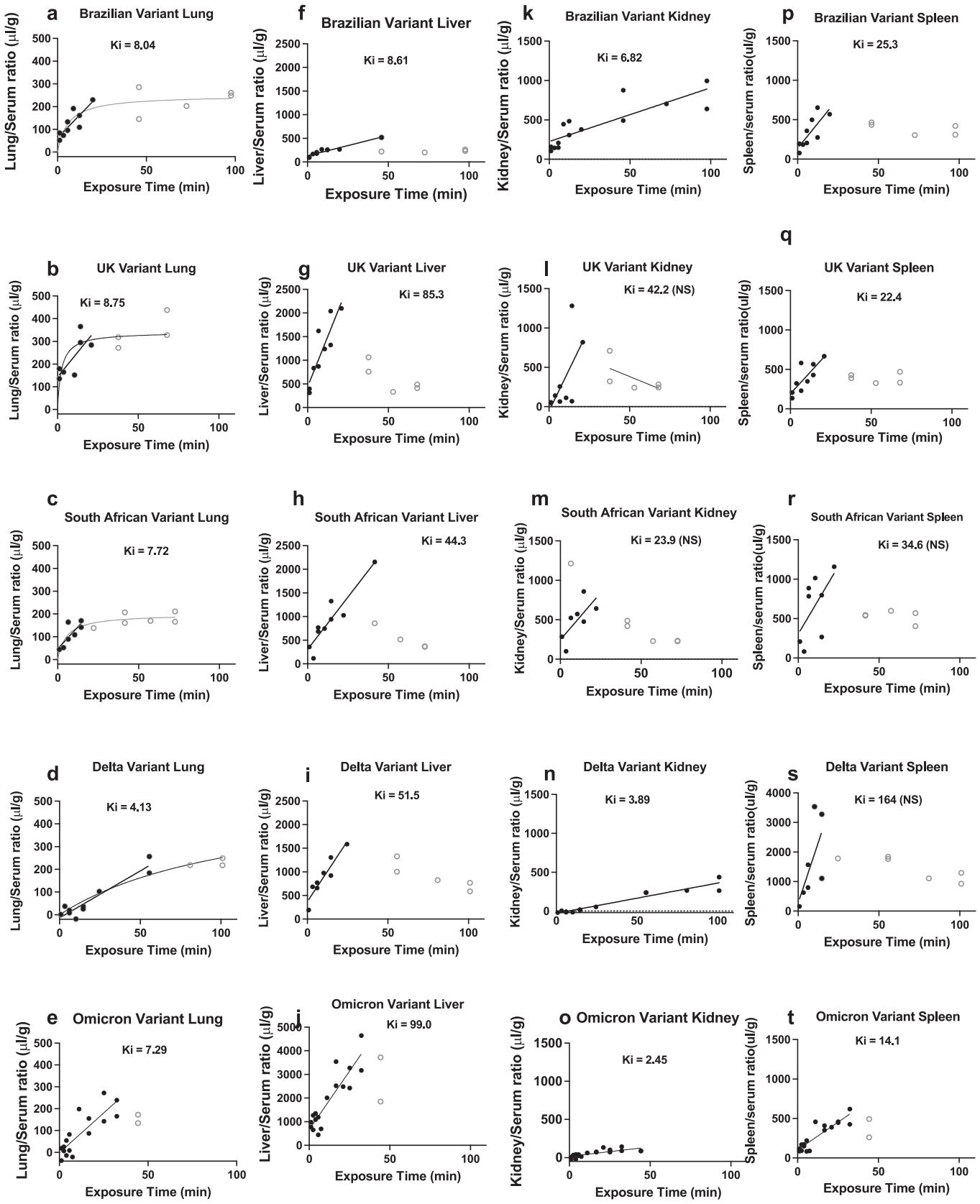

Fig. 5. Uptake of intravenously administered S1 variants by peripheral tissues. Unidirectional influx constants (Ki, in units of µl/g-min) for the various tissues and variants are shown. The relation between tissue/serum ratios and exposure time was statistically significant for all combinations except the Delta variant and South African uptakes by spleen and the South African and UK uptakes by kidney. Closed circles used in calculations of linearities; open circles departed from linearity and so were not included in calculations of Ki.

development of antibodies directed against the S protein. We, therefore, examined the effect of some available S protein antibodies on the blood clearance, BBB penetration, and peripheral tissue uptake of S1. The blocking antibodies AX290 and AX677 decreased the brain/serum ratios for S1 and AX290 decreased the percent of the injected dose taken up by brain. However, antibodies can have variable effects on clearance of their ligands and here AX290 and AX677 increased blood levels of S1. Such increases in blood levels are typically caused by decreased clearance rates or by reducing the volume of distribution. We found an increase in the tissue/serum ratio of S1 for kidney, but not for liver, suggesting that clearance was increased, rather than decreased by antibody binding. AX290 and AX677 also increased tissue/serum ratios for lung and spleen, but not for liver. The Proteintech antibody decreased the %Inj/ml for I-S1, consistent with increased clearance of S1 from blood (Fig. 6n). The tissue/serum ratio reflects the uptake rate and was increased for kidney (Fig. 6q), but unaffected for brain, liver, lung,

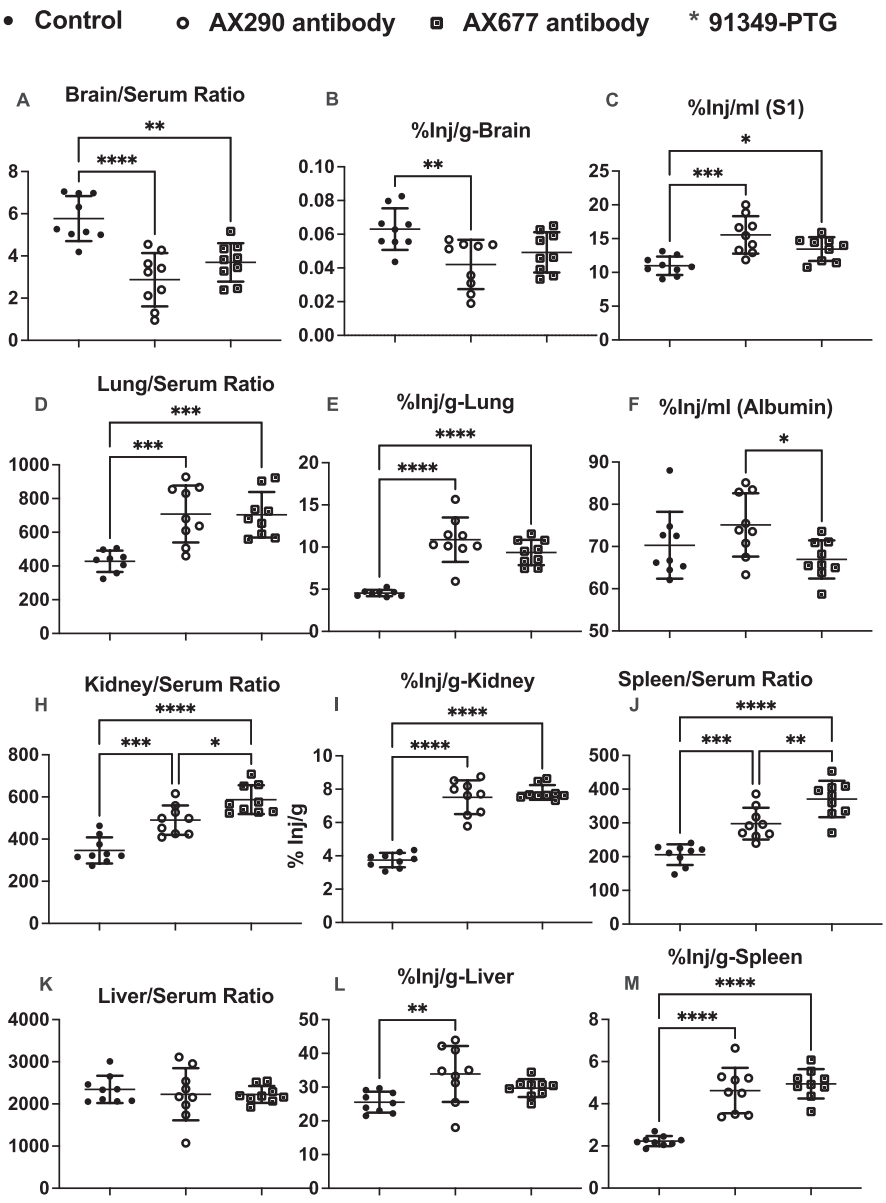

Fig. 6. Effects of antibodies on I-S1 Kinetics. Tissue/serum ratios are in units of. µl/g. Brain uptake of I-S1 as measured by brain /serum ratios ($F(2,24) = 16.9$, $p < 0.0001$) was blocked by AX290 ($p < 0.0001$) and by AX677 ($p = 0.0013$) and as measured by %Inj/g ($F(2,24) = 6.04$, $p = 0.0075$) was blocked by AX290 ($p = 0.0061$). CIearance of I-S1 from blood as measured by %Inj/ml ($F(2,24) = 11.2$, $p = 0.0004$) was decreased by AX290 ($p = 0.0002$) and by AX677 ($p = 0.04$). Lung uptake as measured by lung/serum ratios ($F(2,24) = 12.3$, $p = 0.0002$) was increased by AX290 ($p = 0.0006$) and by AX677 ($p = 0.0008$) and as measured by %Inj/g ($F(2,24) = 28.2$, $p < 0.0001$) was increased by AX290 ($p < 0.0001$) and by AX677 ($p < 0.0001$). Kidney uptake as measured by kidney/serum ratios ($F(2,24) = 29.7$, $p < 0.0001$) was increased by AX290 ($p = 0.0004$) and by AX677 ($p < 0.0001$) and as measured by %Inj/g ($F(2,24) = 97.9$, $p < 0.0001$) was increased by AX290 ($p < 0.0001$) and by AX677 ($p < 0.0001$). Spleen uptake as measured by spleen/serum ratios ($F(2,24) = 30.4$, $p < 0.0001$) was increased by AX290 ($p = 0.0006$) and by AX677 ($p < 0.0001$) and as measured by %Inj/g ($F(2,24) = 34.9$, $p < 0.0001$) was increased by AX290 ($p < 0.0001$) and by AX677 ($p < 0.001$). Liver uptake as measured by %Inj/g ($F(2,24) = 5.51$, $p = 0.011$) was increased by AX290 ($p = 0.008$).The Proteintech antibody 91349-PTG decreased the %Inj/ml of I-S1 ($t = 3.40$, $df = 18$, $p = 0.0032$) and increased the kidney/serum ratio ($t = 2.58$, $df = 18$, $p = 0.019$), consistent with antibody-induced enhanced renal clearance of S1. No other tissue/serum ratio was altered. The uptake of I-S1 as measured by the %Inj/g-tissue was decreased for brain ($t = 2.56$, $df = 18$, $p = 0.019$), liver ($t = 2.33$, $df = 18$, $p = 0.032$), and spleen ($t = 2.94$, $df = 18$, $p = 0.0088$), but not lung or kidney. *$p < 0.05$; **$p < 0.01$; ***$p < 0.001$; ****$p < 0.0001$.

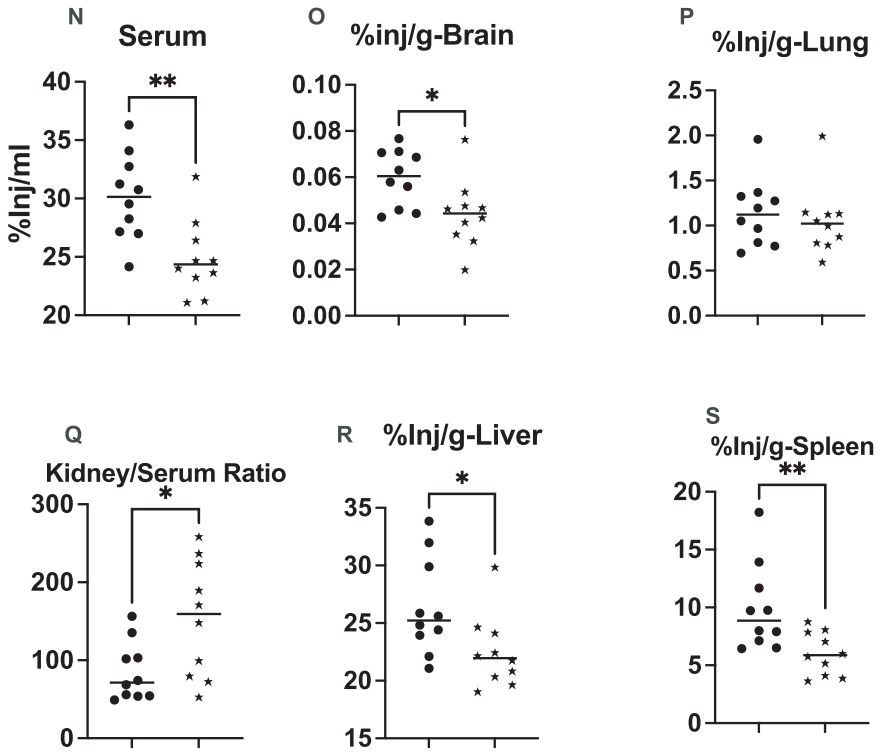

Fig. 6. (*continued*).

or spleen, suggesting that the antibody enhanced S1 clearance by the kidney. The %Inj/g which is dependent on both tissue uptake rate and the clearance rate from blood was decreased for brain, spleen, and liver, but not lung (Fig. 6o, p,r,s) or kidney. Taken together, these results suggest that one mechanism by which antibodies decrease tissue uptake of S1 is by increasing renal clearance, which in turn lowers blood levels and so reduces the amount of S1 available for uptake by the nonrenal tissues. The R&D antibody had no statistically significant effect on I-S1 clearance or tissue uptakes.

3.6. ICV injection of SARS-PV induces neuroinflammation

We tested the possibility that SARS-CoV-2 once in brain can induce inflammation even in the absence of productive infection. SARS-PV four days after its icv injection could be visualized by staining for GFP, demonstrating that it had been internalized by brain cells (Fig. 7a vs 7e). Iba1 and GFAP staining showed that microglia and astrocytes were activated, respectively (Fig. 7b vs 7f, 7c vs 7 g). The inflammatory region as assessed by Iba1 and GFAP staining extended beyond the region of viral uptake as assessed by GFP staining (Fig. 7d), indicating that viral incorporation into the cellular genome was not the only mechanism of inflammation. RNAscope found evidence for viral uptake only in microglial cells Fig. 7i), but not astrocytes (Fig. 7j), neurons (Fig. 7k) or endothelial cells (Fig. 7l). The reactive microgliosis suggests that SARS-PV induces neuroinflammation by being taken up by those cells, but the astrogliosis shows that there are also mechanisms that do not involve incorporation of the viral genome. Viral or S protein binding and/or internalization without subsequent incorporation into the cells' genome is likely sufficient to induce a neuroinflammatory response in the cells of the NVU, including microglia, astrocytes, neurons, pericytes, and brain endothelial cells. Release of cytokines would also be a mechanism by which one inflamed cell could induce inflammation in another and so we then determined whether icv S1 could induce cytokine release in brain.

3.7. Neuroinflammation induced by ICV injection of S1 is greatest in the aged SAMP8 mouse model of Alzheimer's disease

Risk factors associated with the acquisition and severity of COVID-19 and the risk for developing Long COVID include sex, age, obesity, and Alzheimer's disease. Here, we determined whether these risk factors affected the ability of S1 injected into the CNS to induce neuroinflammation as measured by cytokine levels. We first tested the ability of ip S1 administered to young CD-1 males to induce cytokine release in blood. IP injection of 10 μg/mouse of S1 into 2 mo old male CD-1 mice resulted in no changes in brain levels of the cytokines and statistically significant increases in serum IL-3 and TNF (Fig. 8a-b). ICV injection of S1 (0.01, 0.1, or 1.0 μg/mouse) into 2 mo old male CD-1 mice resulted in no changes of any cytokine in the blood and no change in body weight. ICV injection of 0.01 μg/mouse (young CD-1 males) of S1 decreased brain levels of IL-5 (Fig. 8c). All doses of S1 decreased GM-CSF levels (Fig. 8d). The 1.0 μg/mouse of S1 increased brain levels of IL-12(p40) and RANTES [$F(3,35) = 16.1$, $p < 0.0001$] (Fig. 8e-f). ANOVA also showed a difference for MIP-1 alpha, but with no post-test differences. As the icv pattern of cytokine release is remarkably different from that seen after ip injection, the results of the icv study must be due to direct action within the brain and cannot be ascribed to S1 stimulation of peripheral events from brain S1 leaking into the blood.

ICV injection of 1.0 μg/mouse of S1 into young and aged male and female CD-1 mice only showed an effect on RANTES, increasing levels of brain RANTES in young males ($p = 0.016$), old males ($p < 0.0001$) and young females ($p = 0.032$), but not in aged females (Fig. 9a). Sex or age influenced levels of five brain cytokines: IL-5 was reduced in females compared to males (Fig. 9b), IL-6 (Fig. 9c), MCP-1 (Fig. 9d), MIP-1 beta (Fig. 9e), and MIP-1 alpha (Fig. 9f) were higher in older than younger females. However, there was no interaction of either sex or age with S1 treatment. We conclude that in CD-1 mice, S1 had minimal effects on brain cytokines and that effect was not altered by sex or age.

Both Alzheimer's disease and amyloid beta peptide have been associated with worse outcomes to SARS-CoV-2 infections. Epidemiological

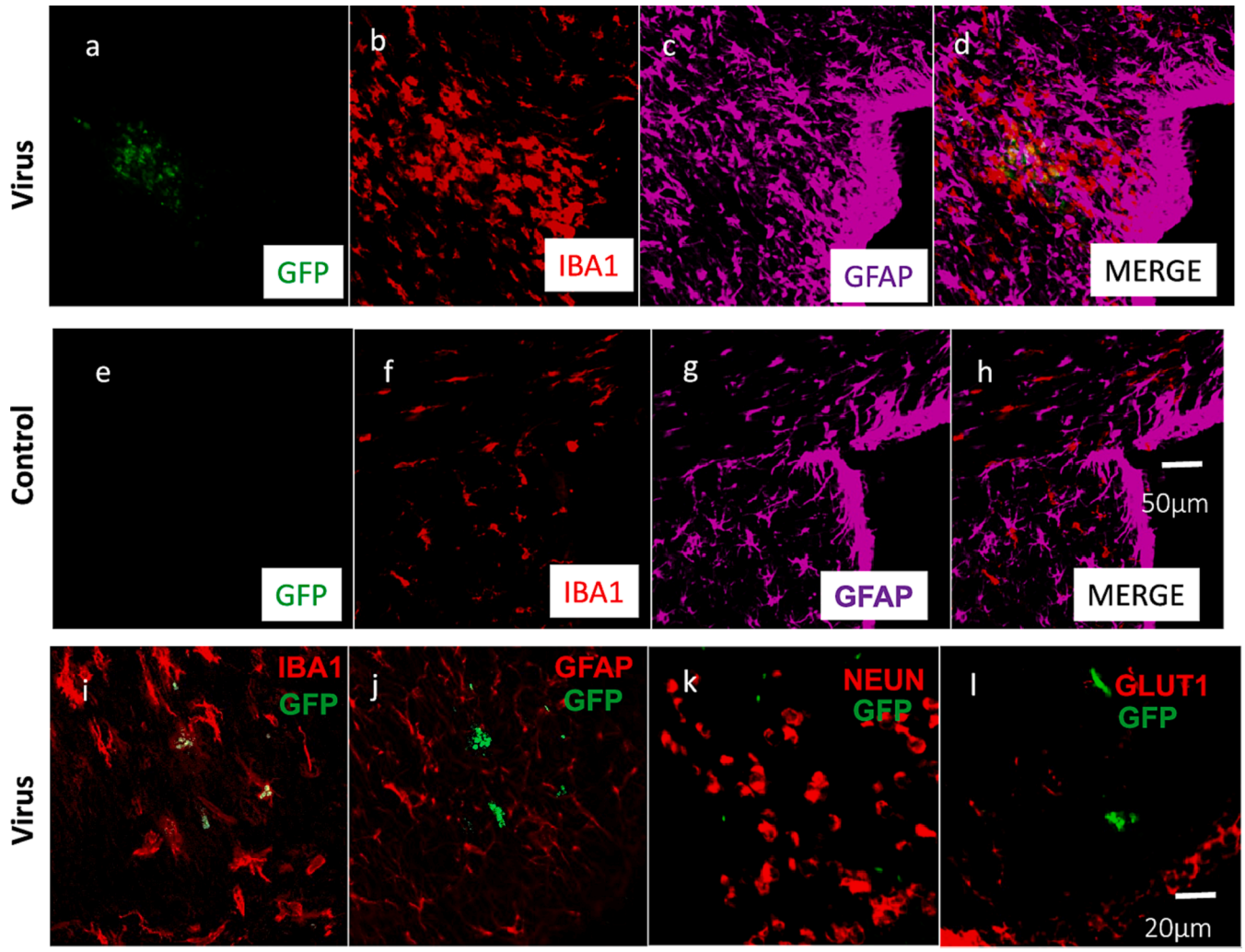

Fig. 7. ICV SARS-PV is taken up by microglia and induces neuroinflammation. Four days after icv injection of GFP containing SARS-PV, **a** (in contrast to vehicle injection in **e**) shows uptake by brain tissue, with induction of inflammation by microglia (**b** vs **f**) and astrocytes (**c** vs **g**). The area of inflammation appeared to extend beyond the area of viral uptake (**d**) consistent with direct and indirect mechanisms of viral-induced inflammation. RNAscope showed GFP virus co-localizing with microglia (**i**), but no co-localization with astrocytes (**j**), neurons (**k**), or endothelial cells (**l**).

studies show that some of the worsened outcomes for COVID-19 in Alzheimer's disease patients is ascribable to the increase in amyloid beta peptide (Chiricosta et al., 2021). Although amyloid beta peptide can have anti-viral properties (Bourgade et al., 2015), in the case of SARS-CoV-2 it aids infections by facilitating binding between ACE2 and the S protein, enhancing cell uptake (Hsu et al., 2021; Idrees and Kumar, 2021). Here, we examined the effect of ICV S1 on brain cytokine levels in young and aged SAMP8 mice, a mouse model of Alzheimer's disease. The SAMP8 is a strain that with aging develops cognitive defects, increases in brain levels of amyloid precursor protein (APP) and amyloid beta peptide, and oxidative stress in brain, all reversible with antisense directed against APP (Morley et al., 2002). The SAMP8 set of mice consisted of male mice that were young (2 mo),), an age prior to the onset of amyloid beta accumulation and cognitive decline, or aged (12 mo), when amyloid beta accumulation and cognitive impairment are present (Flood and Morley, 1998). In comparison to CD-1 mice, SAMP8 mice had a very robust response to S1 (Fig. 10). Four cytokines were increased in brain: IL-12(p40), MIP-1alpha, MIP-1beta, and RANTES (Fig. 10a, d-f). The response was more robust in older mice for each of these cytokines and, additionally, eotaxin was increased only in older mice (Fig. 10a,b, d-f). Aging alone had suppressive effects on IL-1beta and IL-13 in mice not treated with S1 and on IL-17 in mice treated with S1 (Fig. 10g-i). These results strongly support Alzheimer's disease/amyloid beta peptide as modeled by the SAMP8 as risks for increased S1-induced inflammation.

As obesity increases the risk for Alzheimer's disease and is also a risk factor for both acquisition and worse outcomes of COVID-19, we placed some SAMP8 mice on a high fat diet for 8 months, starting at the age of 4 mo. The high fat diet increased body weight by about 40 % (Fig. 10j) and increased serum leptin levels to levels typically seen in obesity (35 ng/ml; Fig. 10*k*). However, modifications by obesity on the influences of S1 on brain cytokines were not robust, with no effects on Il-12(p40), MIP-1 alpha, MIP-1 beta, or RANTES. The increase in eotaxin induced by S1 was not significant in the obese mice, but for KC, S1 induced an increase only in the obese group (Fig. 10c). Injection of S1 icv did not induce weight loss in these mice, consistent with findings by Frank et al (Frank et al., 2022). However, S1 increased serum levels of the orexigenic hormone ghrelin in aged SAMP8, but not in young or aged-high fat SAMP8 mice (Fig. 10*l*) and slightly decreased serum levels of the anorexic hormone leptin in aged mice on high fat diet (Fig. 10*k*). Serum levels of the metabolic hormones insulin, resistin, and PAI-1 were not affected by S1. This is consistent with the sickness behavior induced by SARS-CoV-2 not having the classic feature of anorexia.

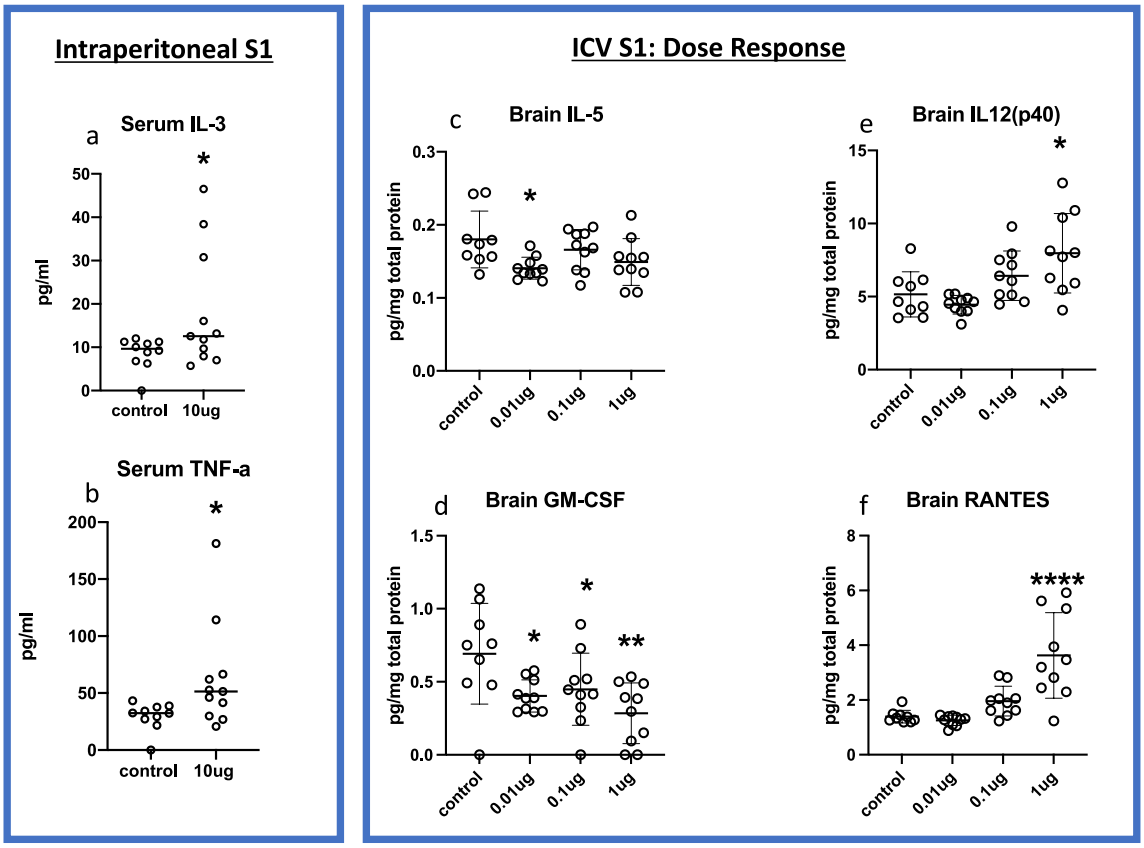

Fig. 8. Intraperitoneal and brain intraventricular injection of S1 releases cytokines in CD-1 mice. Intraperitoneal injection of S1 (10 μg/mouse) increased blood levels of IL-3 (**a**, df = 19, t = 2.09, p = 0.0498) and TNF-alpha (**b**, df = 19, t = 2.19, p = 0.41). A dose response curve of icv S1 showed in brain a decrease in IL-5 a the lowest dose [**c**, F(3,35) = 3.41, p = 0.028], a decrease in GM-CSF at all doses [**d**, F(3,35) = 4.80, p = 0.006], and increases in IL12(p40) [**e**, F(3,35) = 7.20, p = 0.0007] and RANTES [**f**, F(3,35) = 16.1, p < 0.0001] at the highest dose of 1 μg/mouse. *p < 0.05; **p < 0.01; ***p < 0.001; ****p < 0.0001.

3.8. S1 uptake by brain is decreased and by lung is increased in the SAMP8 mouse model of Alzheimer's disease

Interactions between S1 and amyloid beta peptide in the SAMP8 mouse could also result in differences in uptakes by various tissues. Clearance rates of iv injected I-S1 did not differ between young (slope = (-)0.042 ± 0.016 %Inj/ml-min; $t_{1/2}$ = 7.2 min) and aged (slope = (-) 0.027 ± 0.007 %Inj/ml-min; $t_{1/2}$ = 11.1 min) SAMP8 mice (Fig. 11a). Published data (Rhea et al., 2021) for clearance and tissue uptakes in CD-1 male mice are shown for comparison as dashed lines and for clearance did not differ from the SAMP8 groups. The transport rate across the BBB in young and aged SAMP8 did not differ from each other, but was slower when compared to the published data for young CD-1 mice (Fig. 11b; p = 0.0006). Uptake rates for young and aged SAMP8 or for the published data for young CD-1 mice did not differ for kidney, spleen, or liver (Fig. 11d-f). The slopes for lung were not significant, indicating that S1 had reached equilibrium between blood and lung. Uptakes did not differ between young and old SAMP8 mice but were about 10 times higher than uptake by lung (Fig. 11c; p < 0.0001). Our previously published data (Rhea et al., 2021) indicated that the murine ACE2 binding site was more important for lung uptake in young CD-1 mice than for any other tissue. The high uptake seen here for lung in the SAMP8 is consistent with reports showing that amyloid beta peptide facilitates binding of S1 and ACE2 (Hsu et al., 2021; Idrees and Kumar, 2021).

3.9. ICV S1 increases amyloid beta peptide in young SAMP8 mice

The effects of acute icv S1 on brain levels of the amyloid beta peptides were tested in young and old CD-1 mice and in young, old, and old obese SAMP8 mice. 24 h after ICV S1, amyloid beta peptide 1–40 (Fig. 12a) was elevated and showed a trend towards elevation of amyloid beta peptide 1–42 (Fig. 12c) in young SAMP8 mice. ICV S1 had no statistically significant effects on amyloid beta peptide levels in young or old CD-1 mice or in aged or aged obese SAMP8 mice.

4. Discussion

How COVID-19 transforms from an acute respiratory disease to one with many CNS manifestations likely involves a variety of mechanisms. That S1 (Rhea et al., 2021) and many of the cytokines released during the cytokine storm of COVID-19 can cross the BBB to induce or enhance neuroinflammation is well established (Banks, 2005). The ability of SARS-CoV-2 to cross the BBB is less well established and its ability to induce neuroinflammation is unexamined. Here, we show that two viral models of SARS-CoV-2, a pseudovirus bearing the S protein and a virus like particle bearing all four viral proteins of SARS-CoV-2, readily cross the BBB of the mouse. Indeed, these two models of SARS-CoV-2 cross 4 times faster than the viral attachment protein S1, suggesting that either the full S protein or conformational advantages of being embedded in the viral membrane facilitates uptake by the BBB. The other three proteins, 2 of which are inserted in the membrane, do not seem to aid in viral transport across the BBB as the VLPs transport rate approximates that of the pseudovirus.

The mechanism by which SARS-PV and VLPs cross the BBB is similar to that of S1 as evidenced by WGA enhancing viral transport across the BBB. Adsorptive transcytosis (transport across the BBB) is the classic method by which viruses enter cells and cross the BBB and depends on interactions between the viral attachment glycoproteins of the virus and the glycoproteins and glycolipids of the targeted cell. The sugars of the

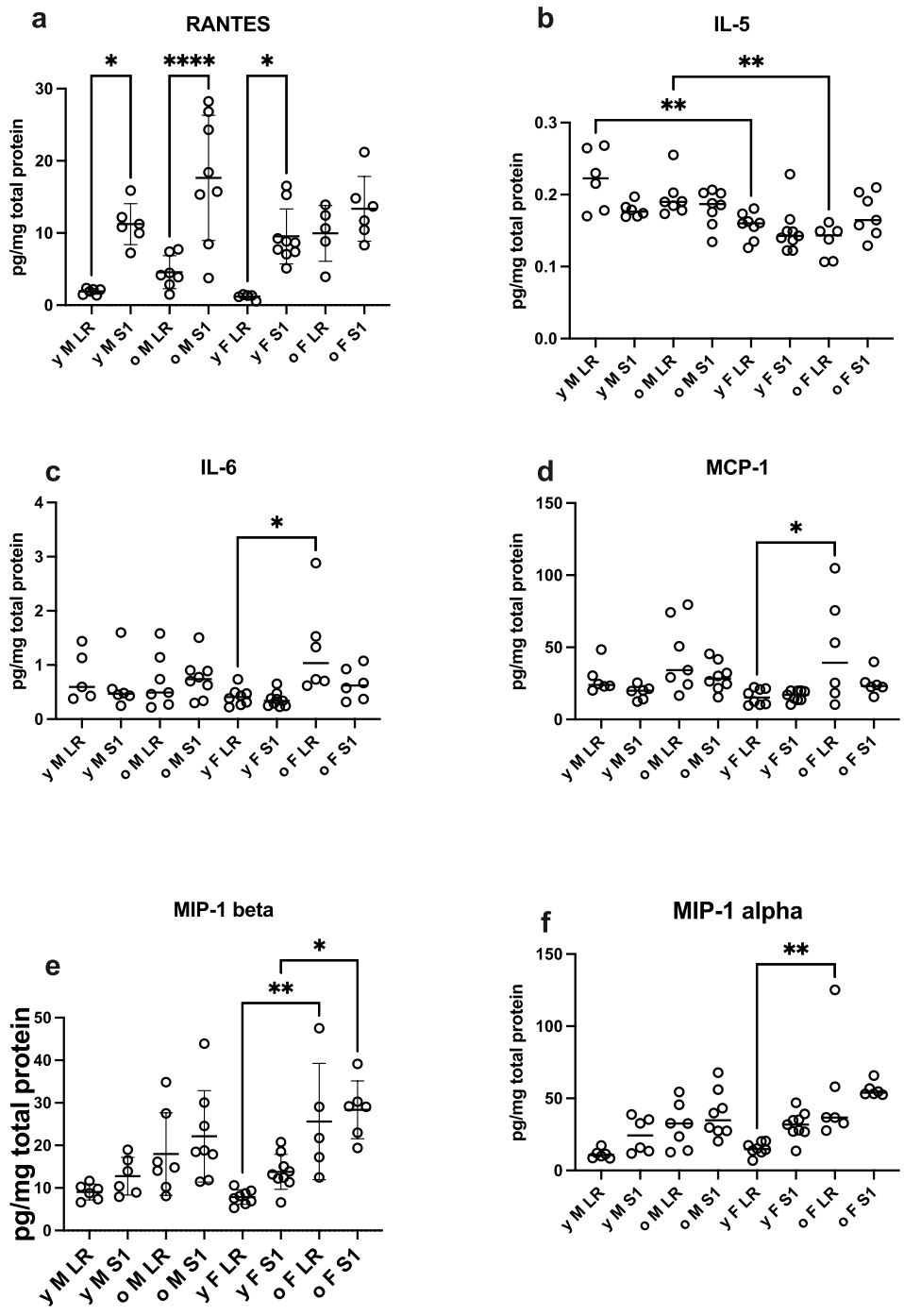

Fig. 9. Effect of ICV S1, sex, and aging on levels of brain cytokines in CD-1 mice. **a**, ICV S1 increased brain levels of RANTES [$F(7,44) = 10.7$, $p < 0.0001$]. ANOVA's showed effects of sex [**b**, IL-5: $F(7,49) = 6.39$, $p < 0.0001$, young male > young female ($p = 0.0017$), old male > old female ($p = 0.0049$)] or age: **c**, IL-6: $F(7,47) = 2.93$, $p = 0.013$, young females < old females ($p = 0.011$)]; **d**, MCP-1: $F(7, 48) = 3.92$, $p = 0.0018$, young females < old females ($p = 0.012$)]; **e**, MIP-1 beta $F(7,47) = 6.67$, $p < 0.0001$, young vs aged female controls ($p = 0.003$), young S1 treated females vs old S1 treated females ($p = 0.012$); **f**, MIP-1 alpha: $F(7, 48) = 6.73$, $p < 0.0001$, young < old female ($p = 0.0013$)]. yMLR = young males given lactated Ringers (vehicle); yMS1 = young males given S1, oMLR = old males given lactated Ringer's, oMS1 = old males given S1, yFLR = young females given lactated Ringer's, yFS1 = young females given S1, oFLR = old females given lactated Ringers, oFS1 = old females given S1. *p < 0.05; **p < 0.01; ***p < 0.001; ****p < 0.0001.

glycoproteins are key to determining these interactions. *N*-acetylglucosamine and mannose, for example, are key to the uptake of HIV-1′s viral attachment protein, gp120 (Dohgu et al., 2012; Mizuochi et al., 1988). Here, stimulation of uptake by lectins gave more robust results than attempts to inhibit uptake by sugars. Both approaches indicate an importance of *N*-acetylglucosamine, *N*-acetylgalactosamine, and mannose for I-S1 uptake by lung. It was surprising that sialic acid was not shown here to be important sugar as its role in SARS-CoV-2 binding to human ACE-2 is well documented (Nguyen et al., 2022). However, SARS-CoV-2 binds murine ACE-2 much less avidly and so our results are likely reflecting S1 binding to other receptors.

The importance of the specific sugars varied among the tissues. For example, *N*-acetylglucosamine played an important role in S1 binding in brain, but not liver or spleen. The lectin results show that brain and lung are more similar to one another in their sugar requirements than to the other tissues. Interestingly, a similar clustering of brain and lung was found for exosome uptake (Banks et al., 2022). These results suggest that more than one site binds SARS-CoV-2 and that those binding sites are heterogeneously distributed among the tissues.

The differences in initial cellular uptake rates and so infection rates among the variants of SARS-CoV-2 is largely dictated by the variations in its S protein. We found that the last two variants, delta and omicron,

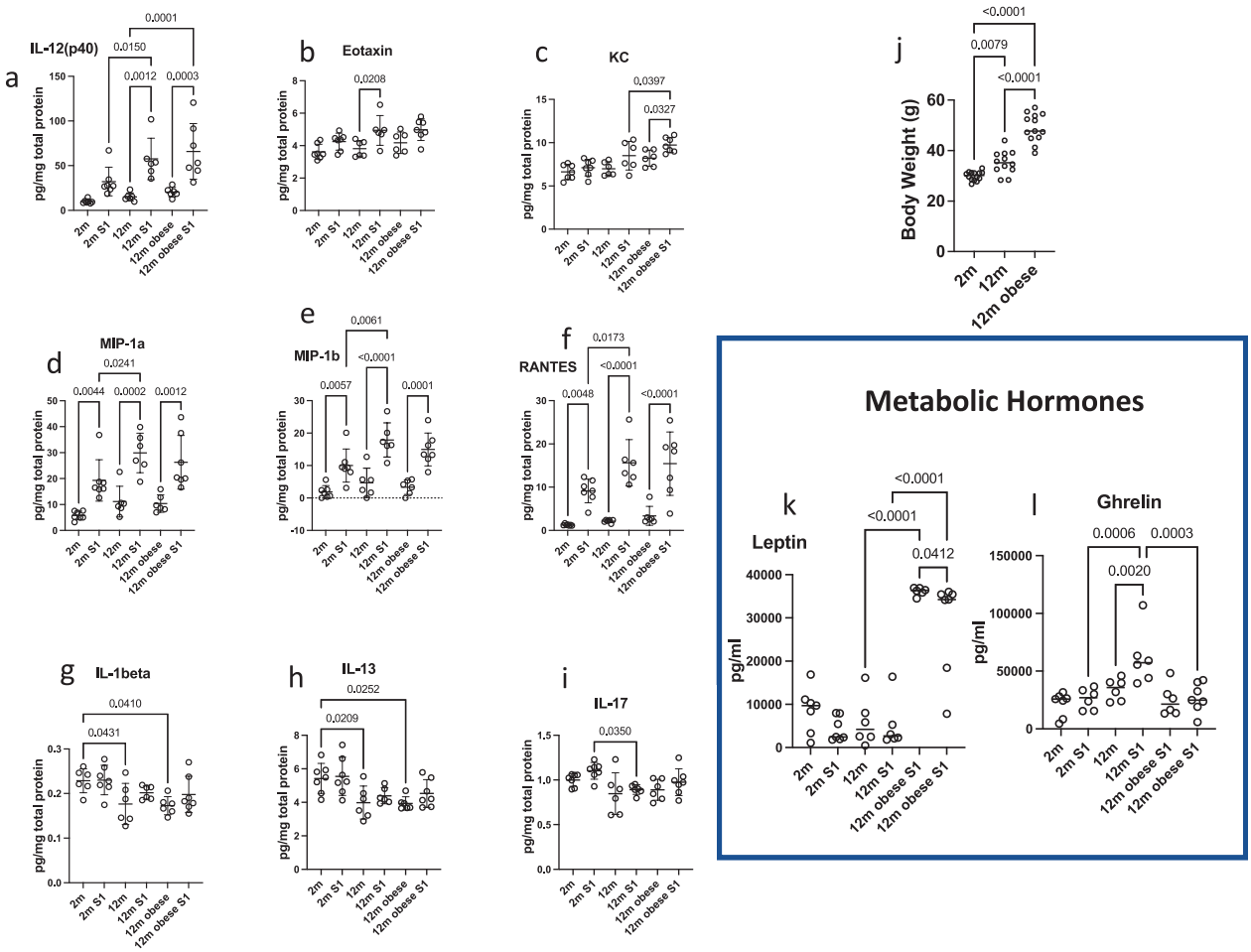

Fig. 10. Effects of SAMP8 strain, aging, and obesity on icv S1-induced increases in brain cytokines. Six groups of male SAMP8 mice were studied: 2 mo old (2 m, n = 7), 2 mo old treated with S1 (2 m S1, n = 7), 12 mo old (12 m, n = 6), 12 mo old treated with S1 (12 m S1, n = 6), 12 mo old obese (12 m obese, n = 6), 12 mo old obese treated with S1 (12 obese S1, n = 7). S1 treatment increased in one or more groups brain levels of (**a**) IL-12p(40) [$F(5,33) = 11.4$, $p < 0.0001$], (**b**) eotaxin [$F(5,33) = 5.26$, $p = 0.0012$], (**c**) KC [$F(5,33) = 8.74$, $p < 0.0001$], (**d**) MIP-1alpha [$F(5, 33) = 12.6$, $p < 0.0001$, **(e)** MIP-1beta [$F(5,33) = 15.3$, $p < 0.0001$, (**f**) RANTES [$F(5,33) = 17.5$, $p < 0.0001$. The increase in brain induced by S1 was greater in older mice for IL-12(p40), MIP-1alpha, MIP-1beta, and RANTES and greater in obese mice for KC. Age was associated with lower brain levels for (**g**) IL-1 beta [$F(5,32) = 3.58$, $p = 0.011$], (**h**) IL-13 [$F(5,33) = 4.52$, $p = 0.0030$], and aged S1-treated mice for (**i**) IL-17 [$F(5,33) = 3.29$, $p = 0.016$]. Body weights (**j**) prior to injection of S1 were 29.9 ± 1.7 g for 2 mo old SAMP8, 35.3 ± 4.6 g for 12 mo old SAMP8, and 49.0 ± 5.6 g for 12 mo old SAMP8 obese (all groups different from one another at $p < 0.01$); S1 did not cause a decrease in body weight of any of the groups. **k**, blood leptin levels in 12 mo old SAMP8 mice on high fat diet (36.2 ± 0.9 ng/ml) was decreased by icv S1 (28.8 ± 11.2 ng/ml): $p < 0.05$ and **I**, blood ghrelin levels in 12 mo SAMP8 mice on a low fat diet (mean ± SD; 34.1 ± 9.4 ng/ml) was increased by icv S1 (61.4 ± 24.1 ng/ml): $p < 0.01$. S1 had no effect on blood levels of PAI, resistin or insulin. m = month.

crossed the BBB about 60 % faster than the South African variant. This would suggest that these variants enter the brain faster than the other variants. The occurrence rates of Long COVID among SARS-CoV-2 variants seems to have been addressed in only one paper which found that Long COVID is about twice as common in the delta variant than in the omicron variant (Antonelli et al., 2022).

The low uptake of S1 by lung and the similar uptake rates among the variants for lung are consistent with ACE2 being the major binding site for lung and murine ACE2 poorly binding to S1. Higher uptake rates for the other peripheral tissues are consistent with other binding sites dominating uptake by liver, kidney, and spleen. Liver and kidney are major clearance sites for proteins in blood and these results show that whereas the liver is the major site for each variant, the kidney is also relevant for the UK, South African, and especially the Brazilian variants. The highest uptake of any variant by any tissue was the uptake of the delta variant by the spleen. Such avid uptake by an immune tissue may have contributed to the delta variants robust clinical symptomatology. The variability among the variants for uptake by the various tissues could likewise account for their variation in symptomatologies (Menni et al., 2022).

We found that S1 blocking antibodies decreased the penetration of S1 into brain either when results were expressed as brain/serum ratios or as the percent of the injected dose entering brain (%Inj/g). These findings are in agreement with in vitro studies in CNS organoids (Song et al., 2021) and BEC monolayers (Krasemann et al., 2022). Brain/serum ratios and %Inj/g describe similar, but distinct, aspects of S1 uptake by brain. The brain/serum ratio is the more pure measure of the rate at which S1 crosses the BBB. The %Inj/g reflects the influence of both the uptake rate and clearance from blood. Binding antibodies can have similar properties to plasma binding proteins. The effects of plasma binding proteins on the uptake of their ligands by various tissues can be varied and complex. For example, by reducing the free fraction of its ligand, binding proteins can reduce uptake by tissues or, by decreasing ligand clearance and so prolonging half-life, binding proteins can result in increased uptake by tissues. Here, AX290 and AX677 increased blood levels of S1, indicating that they prolonged half-life. In comparison, 91349-PTG decreased blood levels of S1, apparently by increasing clearance by kidney. An unexpected finding was that AX290 and AX677 selectively increased the tissue/serum ratios for lung, kidney, and

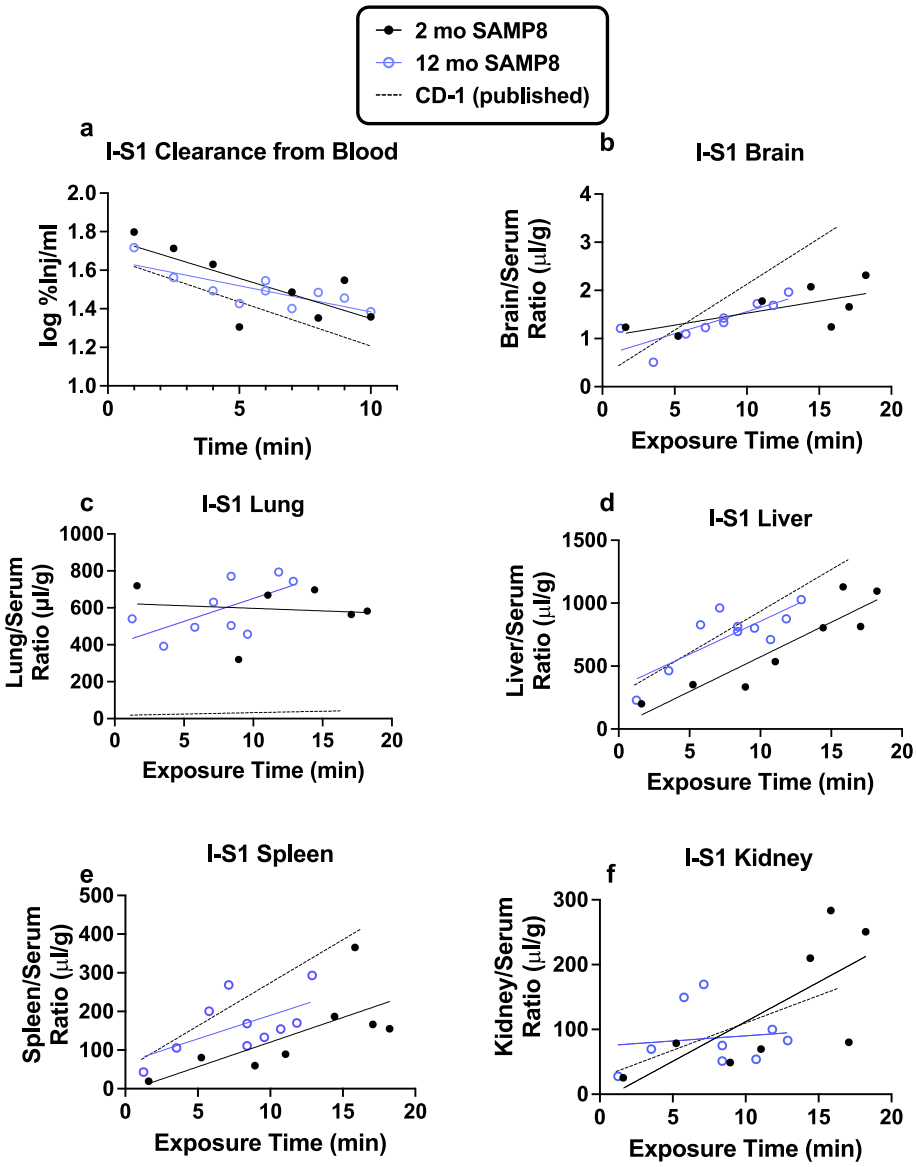

Fig. 11. Clearance and brain and tissue uptakes of I-S1 by young and old male SAMP8 mice. Published values (Rhea et al., 2021) for young male CD-1 are shown as a dashed line for comparison. Slopes for clearance or uptake by liver, spleen, or kidney did not differ between young and old SAMP8 nor with the published CD-1 data. For brain, young SAMP8 uptake rates (Ki = 0.050 ±0.025 µl/g-min, n = 8, r^2 = 0.44; p = 0.1) and aged SAMP8 (Ki = 0.092 ±0.024 µl/g-min, n = 9, r^2 = 0.68; p = 0.006) did not differ from each other, but was lower when compared to the CD-1 published data (Ki = 0.191 ±0.020 µl/g-min, n = 9, r^2 = 0.937; p < 0.0001; F(2,18) = 11.7, p = 0.0006). Uptake of I-S1 did not differ between young vs aged SAMP8 mice for lung, spleen, or kidney, but the y-intercept was lower in young SAMP8 mice for liver (p = 0.0015). I-S1 uptake by lung was dramatically higher in young and aged SAMP8 mice compared to published uptake in young CD-1 mice as shown by a comparison of their y intercepts: F(2,19) = 51.2, p < 0.0001.

spleen, but not for liver, suggesting that antibody binding facilitated the interactions of S1 with the receptors for these tissues.

Our results show that once within the CNS, SARS-PV and S1 can induce neuroinflammation. As neither SARS-PV nor S1 can replicate, these results show that induction of neuroinflammation does not depend on productive infection. The SARS-PV genome was incorporated into microglia as shown by GFP and microglia became inflamed as evidenced by increased Iba1 levels. This is consistent with studies showing uptake of SARS-CoV-2 by immortalized models of human microglia (Jeong et al., 2022). Although microglia do not possess ACE2, it has been shown that S1 binds to microglial TLR2 and TLR4 (Frank et al., 2022). Astrocytes also became reactive as evidenced by elevated GFAP levels, but we found no evidence fnjhor astrocytic internalization of SARS-PV. We assume that SARS-PV, S1, and microglial inflammatory products in the interstitial fluid result in neuroinflammation of astrocytes and probably other cells of the neurovascular unit. This is consistent with the work of Matschke et al who found robust microglial activation in young patients dying of COVID-19 (Matschke et al., 2022).

Risk factors for COVID-19 are being male, increasing age, obesity, and Alzheimer's disease and for Long COVID are being female, aged between 45 and 65, overweight, and Alzheimer's disease (Denson et al., 2021; Gebhard et al., 2020; Jones et al., 2021; Li et al., 2020; Vanichkachorn et al., 2021; Vimercati et al., 2021; Zhang et al., 2020). In young, male CD-1 mice, ip or icv injections produced only minimal elevations in cytokines in blood and brain, respectively. Interestingly, the cytokine pattern in blood after ip injection was different from the cytokine pattern in brain after icv injection, demonstrating that CNS neuroinflammation is not simply a reflection of peripheral inflammation. Aging and sex in CD-1 mice had no influence on S1-induced elevations in brain cytokines, although there were some influences on baseline levels. In contrast, icv S1 increased brain levels of 4 cytokines (IL-12(p40), RANTES, MIP-1 alpha, and MIP-1 beta) in young SAMP8 mice, of 5 cytokines (IL-12(p40), RANTES, MIP-1 alpha, MIP-1 beta, and eotaxin) in aged SAMP8 mice, and five cytokines in aged, obese SAMP8 mice (IL-12(p40), RANTES, MIP-1 alpha, MIP-1 beta, and KC). Additionally, the magnitude of the increase of the 4 cytokines (IL-12(p40), RANTES, MIP-1 alpha, and MIP-1 beta) was greater in aged than in young SAMP8 mice. The SAMP8 mouse develops age-related cognitive impairments that are dependent on rising levels of brain amyloid precursor protein/amyloid beta peptide (Morley et al., 2002). These results are, therefore, consistent with published results showing that at least some of the risk factors of Alzheimer's disease for COVID-19 are attributable to amyloid precursor protein/amyloid beta peptide (Hsu et al., 2021). Although amyloid beta peptide has some anti-infective

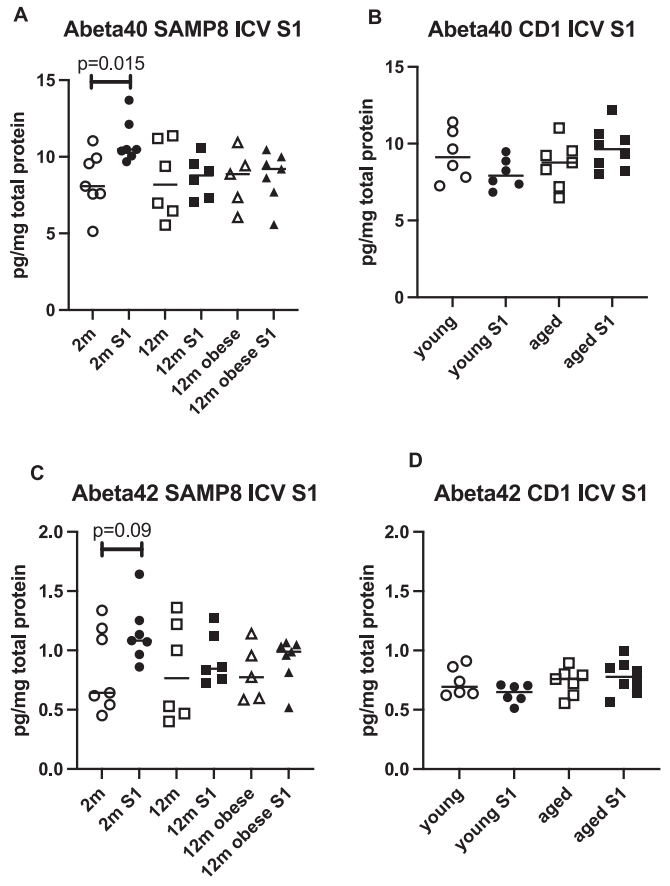

Fig. 12. Effects of ICV S1 on brain levels of the amyloid beta peptides. S1 significantly elevated brain levels of amyloid beta peptide 1–40 in young SAMP8 mice, but not in young or old CD-1 mice or in old or old obese SAMP8 mice. S1 had no statistically significant effects on amyloid beta peptide 1–42 in any of these groups, although there was a statistical trend for its elevation in young SAMP8 mice. m = month.

properties, it promotes COVID-19 by facilitating S protein binding to ACE2 and enhancing viral internalization. An effect of obesity on response to S1 was only seen for KC, which was released only in obese, aged SAMP8 mice. Overall, these results show that age, sex, and obesity in our models have no to minimal effects on S1-induced neuroinflammation as measured by cytokine secretion, but that the SAMP8 phenotype, likely due to its age-related increases in amyloid precursor protein/amyloid beta peptide, has a powerful effect on S1-induced neuroinflammation.

The effect of the SAMP8 phenotype on tissue uptake of S1 was more varied. Transport into brain was lower than that previously measured in young CD-1 male mice (Rhea et al., 2021). Uptake by lung was dramatically higher in SAMP8 mice than in CD-1 mice, which could be explained by ACE2-amlyoid beta peptide interactions discussed above.

These findings raised the question of whether icv S1 altered brain levels of amyloid beta peptide. Inflammation is known to increase amyloid beta peptide levels in brain and to reduce its clearance from brain (Jaeger et al., 2009; Sheng et al., 2003). Here, we found that icv S1 enhanced amyloid beta peptide 40 with a trend towards enhancement of amyloid beta peptide 42 in young SAMP8 mice, but not in the other groups tested. This is consistent with clinical studies that found minimal effects on amyloid beta peptide in patients with COVID-19 (Frontera et al., 2022). This suggests that increases in amyloid beta peptide are not a major feature in the acute inflammation induced by icv S1. However, the results do suggest that amyloid beta peptide can be affected and under other conditions, perhaps such as prolonged inflammation, more significant elevations in amyloid beta peptide might occur. In particular, interactions among ApoE genotypes, amyloid beta peptide, and SARS-CoV-2/COVID-19 seem to occur (Kurki et al., 2021). This study has the following limitations. While our results support detrimental CNS effects of SARS-CoV-2 and S1 independent of viral replication, these effects would likely be more profound if virus replicates in brain. In addition, we recognize species differences in neuroinflammatory responses (Zschaler et al., 2014), especially as mouse ACE-2 interacts very little with S1. Finally, although we studied some factors such as aging, sex, and obesity, humans are exposed to environmental modifiers that were not replicated here (Sundberg and Schofield, 2018).

In conclusion, our results here support the ability of SARS-CoV-2 as assessed by two viral models to cross the BBB by the mechanism of adsorptive transcytosis and to induce neuroinflammation. The S protein is responsible for passage and is also able to induce neuroinflammation. The S1 proteins from the viral variants of concern differ in their rates of uptake by brain and peripheral tissues with the delta and omicron variants showing the most robust uptake by brain. Sex, age, and obesity have minimal effects on S1-induced neuroinflammation, but the SAMP8 phenotype is associated with a robust S1-induced neuroinflammation, likely due to its age-related increases in APP/amyloid beta peptide expression. These results taken together support the concept that SARS-CoV-2 once within the CNS can induce neuroinflammation, even in the absence of productive infection, and that this neuroinflammation could explain associated CNS symptoms including cognitive impairments.

Funding

This work was supported by the VAPSHCS (W.A.B. and M.A.E.) and research grant awards from the National Institutes of Health (R21 AG065928-01 to M.A.E., R21 AG065914 to J.R., and RF-1 AG059088 to W.A.B. and J.R.). We thank AXON COVIDAX a. s.; Bratislava, Slovakia for the AX290 and AX677 antibodies.

Declaration of Competing Interest

The authors declare that they have no known competing financial interests or personal relationships that could have appeared to influence the work reported in this paper.

Data availability

Data will be made available on request.

References

Antonelli, M., Pujol, J.C., Spector, T.D., Ourselin, S., Steves, C.J., 2022. Risk of long COVID associated with delta versus omicron variants of SARS-CoV-2. Lancet 399, 2263–2264.
Banks, W.A., 2005. Blood-brain barrier transport of cytokines: A mechanism for neuropathology. Curr. Pharm. Des. 11, 973–984.
Banks, W.A., Erickson, M.A., 2022. The next chapter for COVID-19: A respiratory virus inflames the brain. Brain Behav. Immun. 101, 286–287.
Banks, W.A., Farr, S.A., La Scola, M.E., Morley, J.E., 2001. Intravenous human interleukin-1 alpha impairs memory processing in mice: Dependence on blood-brain barrier transport into posterior division of the septum. J. Pharmacol. Exp. Ther. 299, 536–541.
Banks, W.A., Sharma, P., Hansen, K.M., Ludwig, N., Whiteside, T.L., 2022. Characteristics of Exosomes and the Vascular Landscape Regulate Exosome Sequestration by Peripheral Tissues and Brain. Int. J. Mol. Sci. 23, 12513.
Baysal, Ö., Abdul Ghafoor, N., Silme, R.S., Ignatov, A.N., Kniazeva, V., 2021. Molecular dynamics analysis of N-acetyl-D-glucosamine against specific SARS-CoV-2's pathogenicity factors. PLoS One 16, e0252571.
Blomberg, B., Mohn, K.G., Brokstad, K.A., Zhou, F., Linchausen, D.W., Hansen, B.A., Lartey, S., Onyango, T.B., Kuwelker, K., Sævik, M., Bartsch, H., Tøndel, C., Kittang, B.R., Cox, R.J., Langeland, N., 2021. Long COVID in a prospective cohort of home-isolated patients. Nat. Med. 27, 1607–1613.
Bourgade, K., Garneau, H., Giroux, G., Le Page, A.Y., Bocti, C., Dupuis, G., Frost, E.H., Fülöp Jr., T., 2015. β-Amyloid peptides display protective activity against the human Alzheimer's disease-associated herpes simplex virus-1. Biogerontology 16, 85–98.
Buzhdygan, T.P., DeOre, B.J., Baldwin-Leclair, A., Bullock, T.A., McGary, H.M., Khan, J. A., Razmpour, R., Hale, J.F., Galie, P.A., Potula, R., Andrews, A.M., Ramirez, S.H., 2020. The SARS-CoV-2 spike protein alters barrier function in 2D static and 3D

microfluidic in-vitro models of the human blood-brain barrier. Neurobiol. Dis. 146, 105131.
Chiricosta, L., Gugliandolo, A., Mazzon, E., 2021. SARS-CoV-2 Exacerbates Beta-Amyloid Neurotoxicity, Inflammation and Oxidative Stress in Alzheimer's Disease Patients. Int. J. Mol. Sci. 22.
Davis, H.E., Assaf, G.S., McCorkell, L., Wei, H., Low, R.J., Re'em, Y., Redfield, S., Austin, J.P., Akrami, A., 2021. Characterizing long COVID in an international cohort: 7 months of symptoms and their impact. EClinicalMedicine 38, 101019.
Denson, J.L., Gillet, A.S., Zu, Y., Brown, M., Pham, T., Yoshida, Y., Mauvais-Jarvis, F., Douglas, I.S., Moore, M., Tea, K., Wetherbie, A., Stevens, R., Lefante, J., Shaffer, J.G., Armaignac, D.L., Belden, K.A., Kaufman, M., Heavner, S.F., Danesh, V.C., Cheruku, S.R., St Hill, C.A., Boman, K., Deo, N., Bansal, V., Kumar, V.K., Walkey, A. J., Kashyap, R., 2021. Metabolic Syndrome and Acute Respiratory Distress Syndrome in Hospitalized Patients With COVID-19. JAMA Netw. Open 4, e2140568.
Dohgu, S., Ryerse, J.S., Robinson, S.M., Banks, W.A., 2012. Human immunodeficiency virus-1 uses the mannose-6-phosphate receptor to cross the blood-brain barrier. PLoS One 7, e39565.
Flood, J.F., Morley, J.E., 1998. Learning and memory in the SAMP8 mouse. Neurosci. Biobehav. Rev. 22, 1–20.
Frank, M.G., Nguyen, K.H., Ball, J.B., Hopkins, S., Kelley, T., Baratta, M.V., Fleshner, M., Maier, S.F., 2022. SARS-CoV-2 spike S1 subunit induces neuroinflammatory, microglial and behavioral sickness responses: Evidence of PAMP-like properties. Brain Behav. Immun. 100, 267–277.
Frontera, J.A., Boutajangout, A., Masurkar, A.V., Betensky, R.A., Ge, Y., Vedvyas, A., Debure, L., Moreira, A., Lewis, A., Huang, J., Thawani, S., Balcer, L., Galetta, S., Wisniewski, T., 2022. Comparison of serum neurodegenerative biomarkers among hospitalized COVID-19 patients versus non-COVID subjects with normal cognition, mild cognitive impairment, or Alzheimer's dementia. Alzheimers Dement. 18, 899–910.
Gebhard, C., Regitz-Zagrosek, V., Neuhauser, H.K., Morgan, R., Klein, S.L., 2020. Impact of sex and gender on COVID-19 outcomes in Europe. Biol. Sex Differ. 11, 29.
Hampshire, A., Trender, W., Chamberlain, S.R., Jolly, A.E., Grant, J.E., Patrick, F., Mazibuko, N., Williams, S.C., Barnby, J.M., Hellyer, P., Mehta, M.A., 2021. Cognitive deficits in people who have recovered from COVID-19. EClinicalMedicine, 101044.
Hascup, E.R., Hascup, K.N., 2020. Does SARS-CoV-2 infection cause chronic neurological complications? Geroscience 42, 1083–1087.
Hsu, J.T., Tien, C.F., Yu, G.Y., Shen, S., Lee, Y.H., Hsu, P.C., Wang, Y., Chao, P.K., Tsay, H.J., Shie, F.S., 2021. The Effects of Aβ(1–42) Binding to the SARS-CoV-2 Spike Protein S1 Subunit and Angiotensin-Converting Enzyme 2. Int. J. Mol. Sci. 22.
Idrees, D., Kumar, V., 2021. SARS-CoV-2 spike protein interactions with amyloidogenic proteins: Potential clues to neurodegeneration. Biochem. Biophys. Res. Commun. 554, 94–98.
Jaeger, J.B., Dohgu, S., Lynch, J.L., Fleegal-DeMotta, M.A., Banks, W.A., 2009. Effects of lipopolysaccharide on the blood-brain barrier transport of amyloid beta protein: A mechanism for inflammation in the progression of Alzheimer's disease. Brain Behav. Immun. 23, 507–517.
Jeong, G.U., Lyu, J., Kim, K.D., Chung, Y.C., Yoon, G.Y., Lee, S., Hwang, I., Shin, W.H., Ko, J., Lee, J.Y., Kwon, Y.C., 2022. SARS-CoV-2 Infection of Microglia Elicits Proinflammatory Activation and Apoptotic Cell Death. Microbiol. Spectr. 10, e0109122.
Jones, R., Davis, A., Stanley, B., Julious, S., Ryan, D., Jackson, D.J., Halpin, D.M.G., Hickman, K., Pinnock, H., Quint, J.K., Khunti, K., Heaney, L.G., Oliver, P., Siddiqui, S., Pavord, I., Jones, D.H.M., Hyland, M., Ritchie, L., Young, P., Megaw, T., Davis, S., Walker, S., Holgate, S., Beecroft, S., Kemppinen, A., Appiagyei, F., Roberts, E.J., Preston, M., Hardjojo, A., Carter, V., van Melle, M., Price, D., 2021. Risk Predictors and Symptom Features of Long COVID Within a Broad Primary Care Patient Population Including Both Tested and Untested Patients. Pragmat. Obs. Res. 12, 93–104.
Kim, E.S., Jeon, M.T., Kim, K.S., Lee, S., Kim, S., Kim, D.G., 2021. Spike Proteins of SARS-CoV-2 Induce Pathological Changes in Molecular Delivery and Metabolic Function in the Brain Endothelial Cells. Viruses 13.
Kovacech, B., Fialova, L., Filipcik, P., Skrabana, R., Zilkova, M., Paulenka-Ivanovova, N., Kovac, A., Palova, D., Rolkova, G.P., Tomkova, K., Csokova, N.T., Markova, K., Skrabanova, M., Sinska, K., Basheer, N., Majerova, P., Hanes, J., Parrak, V., Prcina, M., Cehlar, O., Cente, M., Piestansky, J., Fresser, M., Novak, M., Slavikova, M., Borsova, K., Cabanova, V., Brejova, B., Vinař, T., Nosek, J., Klempa, B., Eyer, L., Hönig, V., Palus, M., Ruzek, D., Vyhlidalova, T., Strakova, P., Mrazkova, B., Zudova, D., Koubkova, G., Novosadova, V., Prochazka, J., Sedlacek, R., Zilka, N., Kontsekova, E., 2022. Monoclonal antibodies targeting two immunodominant epitopes on the Spike protein neutralize emerging SARS-CoV-2 variants of concern. EBioMedicine 76, 103818.
Krasemann, S., Haferkamp, U., Pfefferle, S., Woo, M.S., Heinrich, F., Schweizer, M., Appelt-Menzel, A., Cubukova, A., Barenberg, J., Leu, J., Hartmann, K., Thies, E., Littau, J.L., Sepulveda-Falla, D., Zhang, L., Ton, K., Liang, Y., Matschke, J., Ricklefs, F., Sauvigny, T., Sperhake, J., Fitzek, A., Gerhartl, A., Brachner, A., Geiger, N., König, E.M., Bodem, J., Franzenburg, S., Franke, A., Moese, S., Müller, F. J., Geisslinger, G., Claussen, C., Kannt, A., Zaliani, A., Gribbon, P., Ondruschka, B., Neuhaus, W., Friese, M.A., Glatzel, M., Pless, O., 2022. The blood-brain barrier is dysregulated in COVID-19 and serves as a CNS entry route for SARS-CoV-2. Stem Cell Rep. 17, 307–320.
Kumar, V.B., Farr, S.A., Flood, J.F., Kamlesh, V., Franko, M., Banks, W.A., Morley, J.E., 2000. Site-directed antisense oligonucleotide decreases the expression of amyloid precursor protein and reverses deficits in learning and memory in aged SAMP8 mice. Peptides 21, 1769–1775.
Kurki, S.N., Kantonen, J., Kaivola, K., Hokkanen, L., Mäyränpää, M.I., Puttonen, H., Martola, J., Pöyhönen, M., Kero, M., Tuimala, J., Carpén, O., Kantele, A., Vapalahti, O., Tiainen, M., Tienari, P.J., Kaila, K., Hästbacka, J., Myllykangas, L., 2021. APOE ε4 associates with increased risk of severe COVID-19, cerebral microhaemorrhages and post-COVID mental fatigue: a Finnish biobank, autopsy and clinical study. Acta Neuropathol. Commun. 9, 199.
Li, X., Xu, S., Yu, M., Wang, K., Tao, Y., Zhou, Y., Shi, J., Zhou, M., Wu, B., Yang, Z., Zhang, C., Yue, J., Zhang, Z., Renz, H., Liu, X., Xie, J., Xie, M., Zhao, J., 2020. Risk factors for severity and mortality in adult COVID-19 inpatients in Wuhan. J. Allergy Clin. Immunol. 146, 110–118.
Manzo, C., Serra-Mestres, J., Isetta, M., Castagna, A., 2021. Could COVID-19 anosmia and olfactory dysfunction trigger an increased risk of future dementia in patients with ApoE4? Med. Hypotheses 147, 110479.
Marsh, M., 1984. The entry of enveloped viruses into cells by endocytosis. Biochem. J 218, 1–10.
Matschke, J., Lahann, H., Krasemann, S., Altmeppen, H., Pfefferle, S., Galliciotti, G., Fitzek, A., Sperhake, J.P., Ondruschka, B., Busch, M., Rotermund, N., Schulz, K., Lohr, C., Dottermusch, M., Glatzel, M., 2022. Young COVID-19 Patients Show a Higher Degree of Microglial Activation When Compared to Controls. Front. Neurol. 13, 908081.
Meier, I.B., Vieira Ligo Teixeira, C., Tarnanas, I., Mirza, F., Rajendran, L., 2021. Neurological and mental health consequences of COVID-19: potential implications for well-being and labour force. Brain Commun. 3, fcab012.
Menni, C., Valdes, A.M., Polidori, L., Antonelli, M., Penamakuri, S., Nogal, A., Louca, P., May, A., Figueiredo, J.C., Hu, C., Molteni, E., Canas, L., Österdahl, M.F., Modat, M., Sudre, C.H., Fox, B., Hammers, A., Wolf, J., Capdevila, J., Chan, A.T., David, S.P., Steves, C.J., Ourselin, S., Spector, T.D., 2022. Symptom prevalence, duration, and risk of hospital admission in individuals infected with SARS-CoV-2 during periods of omicron and delta variant dominance: a prospective observational study from the ZOE COVID Study. Lancet 399, 1618–1624.
Miners, S., Kehoe, P.G., Love, S., 2020. Cognitive impact of COVID-19: looking beyond the short term. Alzheimers Res. Ther. 12, 170.
Mizuochi, T., Spellman, M.W., Larkin, M., Solomon, J., Basa, L.J., Feizi, T., 1988. Carbohydrate structures of the human-immunodeficiency-virus (HIV) recombinant envelope glycoprotein gp120 produced in Chinese-hamster ovary cells. Biochem. J 254, 599–603.
Moghimi, N., Di Napoli, M., Biller, J., Siegler, J.E., Shekhar, R., McCullough, L.D., Harkins, M.S., Hong, E., Alaouieh, D.A., Mansueto, G., Divani, A.A., 2021. The Neurological Manifestations of Post-Acute Sequelae of SARS-CoV-2 infection. Curr. Neurol. Neurosci. Rep. 21, 44.
Montagne, A., Barnes, S.R., Sweeney, M.P., Halliday, M.R., Sagare, A.P., Zhao, Z., Toga, A.W., Jacobs, R.E., Liu, C.Y., Amezcua, L., Harrington, M.G., Chui, H.C., Law, M., Zlokovic, B.V., 2015. Blood-brain barrier breakdown in the aging human hippocampus. Neuron 85, 296–302.
Montagne, A., Nation, D.A., Sagare, A.P., Barisano, G., Sweeney, M.D., Chakhoyan, A., Pachicano, M., Joe, E., Nelson, A.R., D'Orazio, L.M., Buennagel, D.P., Harrington, M. G., Benzinger, T.L.S., Fagan, A.M., Ringman, J.M., Schneider, L.S., Morris, J.C., Reiman, E.M., Caselli, R.J., Chui, H.C., Tcw, J., Chen, Y., Pa, J., Conti, P.S., Law, M., Toga, A.W., Zlokovic, B.V., 2020. APOE4 leads to blood-brain barrier dysfunction predicting cognitive decline. Nature 581, 71–76.
Montelaro, R.C., Rueckert, R.R., 1975. On the use of chloramine-T to iodinate specifically the surface proteins of intact enveloped viruses. J. Gen. Virol. 29, 127–131.
Morley, J.E., Farr, S.A., Kumar, V.B., Banks, W.A., 2002. Alzheimer's disease through the eye of a mouse: Acceptance lecture for the 2001 Gayle A. Olson and Richard D. Olson prize. Peptides 23, 589–599.
Morley, J.E., Farr, S.A., Kumar, V.B., Armbrecht, H.J., 2012. The SAMP8 mouse: a model to develop therapeutic interventions for Alzheimer's disease. Curr. Pharm. Des. 18, 1123–1130.
Nation, D.A., Sweeney, M.D., Montagne, A., Sagare, A.P., D'Orazio, L.M., Pachicano, M., Sepehrband, F., Nelson, A.R., Buennagel, D.P., Harrington, M.G., Benzinger, T.L.S., Fagan, A.M., Ringman, J.M., Schneider, L.S., Morris, J.C., Chui, H.C., Law, M., Toga, A.W., Zlokovic, B.V., 2019. Blood-brain barrier breakdown is an early biomarker of human cognitive dysfunction. Nat. Med. 25, 270–276.
Nguyen, L., McCord, K.A., Bui, D.T., Bouwman, K.M., Kitova, E.N., Elaish, M., Kumawat, D., Daskhan, G.C., Tomris, I., Han, L., Chopra, P., Yang, T.J., Willows, S. D., Mason, A.L., Mahal, L.K., Lowary, T.L., West, L.J., Hsu, S.D., Hobman, T., Tompkins, S.M., Boons, G.J., de Vries, R.P., Macauley, M.S., Klassen, J.S., 2022. Sialic acid-containing glycolipids mediate binding and viral entry of SARS-CoV-2. Nat. Chem. Biol. 18, 81–90.
Nuovo, G.J., Suster, D., Awad, H., Michaille, J.J., Tili, E., 2022. The histologic and molecular correlates of liver disease in fatal COVID-19 including with alcohol use disorder. Ann. Diagn. Pathol. 57, 151881.
Pelà, G., Goldoni, M., Solinas, E., Cavalli, C., Tagliaferri, S., Ranzieri, S., Frizzelli, A., Marchi, L., Mori, P.A., Majori, M., Aiello, M., Corradi, M., Chetta, A., 2022. Sex-Related Differences in Long-COVID-19 Syndrome. J. Womens Health (Larchmt) 31, 620–630.
Rhea, E.M., Logsdon, A.F., Hansen, K.M., Williams, L.M., Reed, M.J., Baumann, K.K., Holden, S.J., Raber, J., Banks, W.A., Erickson, M.A., 2021. The S1 protein of SARS-CoV-2 crosses the blood-brain barrier in mice. Nat. Neurosci. 24, 368–378.
Sheng, J.G., Bora, S.H., Xu, G., Borchelt, D.R., Price, D.L., Koliatsos, V.E., 2003. Lipopolysaccharide-induced-neuroinflammation increases intracellular accumulation of amyloid precursor protein and amyloid beta peptide in APPswe transgenic mice. Neurobiol. Dis. 14, 133–145.
Shilatifard, A., Merkle, R.K., Helland, D.E., Welles, J.L., Haseltine, W.A., Cummings, R. D., 1993. Complex-type N-linked oligosaccharides of gp120 from human immunodeficiency virus type 1 contain sulfated N-acetylglucosamine. J. Virol. 67, 943–952.

Silva, J., Patricio, F., Patricio-Martínez, A., Santos-López, G., Cedillo, L., Tizabi, Y., Limón, I.D., 2022. Neuropathological Aspects of SARS-CoV-2 Infection: Significance for Both Alzheimer's and Parkinson's Disease. Front. Neurosci. 16, 867825.
Song, E., Zhang, C., Israelow, B., Lu-Culligan, A., Prado, A.V., Skriabine, S., Lu, P., Weizman, O.E., Liu, F., Dai, Y., Szigeti-Buck, K., Yasumoto, Y., Wang, G., Castaldi, C., Heltke, J., Ng, E., Wheeler, J., Alfajaro, M.M., Levavasseur, E., Fontes, B., Ravindra, N.G., Van Dijk, D., Mane, S., Gunel, M., Ring, A., Kazmi, S.A.J., Zhang, K., Wilen, C.B., Horvath, T.L., Plu, I., Haik, S., Thomas, J.L., Louvi, A., Farhadian, S.F., Huttner, A., Seilhean, D., Renier, N., Bilguvar, K., Iwasaki, A., 2021. Neuroinvasion of SARS-CoV-2 in human and mouse brain. J. Exp. Med. 218.
Steardo Jr., L., Steardo, L., Verkhratsky, A., 2020. Psychiatric face of COVID-19. Transl. Psychiatry 10, 261.
Stefano, G.B., Büttiker, P., Kream, R.M., 2022. Reassessment of the blood-brain barrier: a potential target for viral entry into the immune-privileged brain. Germs 12, 99–101.
Sundberg, J.P., Schofield, P.N., 2018. Living inside the box: environmental effects on mouse models of human disease. Dis. Model. Mech. 11.
Tahira, A.C., Verjovski-Almeida, S., Ferreira, S.T., 2021. Dementia is an age-independent risk factor for severity and death in COVID-19 inpatients. Alzheimers Dement. 17, 1818–1831.
Tangpong, J., Cole, M.P., Sultana, R., Joshi, G., Estus, S., Vore, M., St. Clair, W., Ratanachaiyavong, S., St. Clair, D.K., Butterfield, D.A., 2006. Adriamycin-induced, TNF-alpha-mediated central nervous system toxicity. Neurobiol. Dis. 23, 127–139.
Taquet, M., Dercon, Q., Luciano, S., Geddes, J.R., Husain, M., Harrison, P.J., 2021. Incidence, co-occurrence, and evolution of long-COVID features: A 6-month retrospective cohort study of 273,618 survivors of COVID-19. PLoS Med. 18, e1003773.
Theoharides, T.C., 2022. Could SARS-CoV-2 Spike Protein Be Responsible for Long-COVID Syndrome? Mol. Neurobiol. 59, 1850–1861.
Ushijima, H., Schroder, H.C., Poznanovic, S., Gasic, M.J., Matthes, E., Muller, W.E., 1992. Inhibition of human immunodeficiency virus-1 infection by human conglutinin-like protein: in vitro studies. Jpn. J. Cancer Res. 83, 458–464.
Vanichkachorn, G., Newcomb, R., Cowl, C.T., Murad, M.H., Breeher, L., Miller, S., Trenary, M., Neveau, D., Higgins, S., 2021. Post-COVID-19 Syndrome (Long Haul Syndrome): Description of a Multidisciplinary Clinic at Mayo Clinic and Characteristics of the Initial Patient Cohort. Mayo Clin. Proc. 96, 1782–1791.
Vimercati, L., De Maria, L., Quarato, M., Caputi, A., Gesualdo, L., Migliore, G., Cavone, D., Sponselli, S., Pipoli, A., Inchingolo, F., Scarano, A., Lorusso, F., Stefanizzi, P., Tafuri, S., 2021. Association between Long COVID and Overweight/Obesity. J. Clin. Med. 10.
Wang, Y.F., Chuang, M.H., Chiu, J.S., Cham, T.M., Chung, M.I., 2007. On-site preparation of technetium-99m labeled human serum albumin for clinical application. Tohoku J. Exp. Med. 211, 379–385.
Wang, J., Jiang, M., Chen, X., Montaner, L.J., 2020. Cytokine storm and leukocyte changes in mild versus severe SARS-CoV-2 infection: Review of 3939 COVID-19 patients in China and emerging pathogenesis and therapy concepts. J. Leukoc. Biol. 108, 17–41.
Widmann, C.N., Wieberneit, M., Bieler, L., Bernsen, S., Gräfenkämper, R., Brosseron, F., Schmeel, C., Tacik, P., Skowasch, D., Radbruch, A., Heneka, M.T., 2021. Longitudinal Neurocognitive and Pulmonological Profile of Long COVID-19: Protocol for the COVIMMUNE-Clin Study. JMIR Res. Protoc. 10, e30259.
Xie, Z., Hui, H., Zhao, Z., Yu, W., Wu, R., Zhu, Y., Song, Y., Cao, B., Shi, W., Zhao, D., Zhao, Y., Lv, J., Yao, Q., Duan, Y., Li, J., Zhang, H., Zhou, L., Wang, X., Tian, Y., Zhao, G., 2022. Nervous system manifestations related to COVID-19 and their possible mechanisms. Brain Res. Bull. 187, 63–74.
Yang, R.C., Huang, K., Zhang, H.P., Li, L., Zhang, Y.F., Tan, C., Chen, H.C., Jin, M.L., Wang, X.R., 2022. SARS-CoV-2 productively infects human brain microvascular endothelial cells. J. Neuroinflammation 19, 149.
Zhang, Q., Schultz, J.L., Aldridge, G.M., Simmering, J.E., Kim, Y., Ogilvie, A.C., Narayanan, N.S., 2021b. COVID-19 Case Fatality and Alzheimer's Disease. J. Alzheimers Dis. 84, 1447–1452.
Zhang, J., Wang, X., Jia, X., Li, J., Hu, K., Chen, G., Wei, J., Gong, Z., Zhou, C., Yu, H., Yu, M., Lei, H., Cheng, F., Zhang, B., Xu, Y., Wang, G., Dong, W., 2020. Risk factors for disease severity, unimprovement, and mortality of COVID-19 patients in Wuhan, China. Clin. Microbiol. Infect.
Zhang, L., Zhou, L., Bao, L., Liu, J., Zhu, H., Lv, Q., Liu, R., Chen, W., Tong, W., Wei, Q., Xu, Y., Deng, W., Gao, H., Xue, J., Song, Z., Yu, P., Han, Y., Zhang, Y., Sun, X., Yu, X., Qin, C., 2021a. SARS-CoV-2 crosses the blood-brain barrier accompanied with basement membrane disruption without tight junctions alteration. Signal Transduct. Target. Ther. 6, 337.
Zlokovic, B.V., Begley, D.J., Djuricic, B.M., Mitrovic, D.M., 1986. Measurement of solute transport across the blood-brain barrier in the perfused guinea pig brain: method and application to N- methyl-‡-aminoisobutyric acid. J. Neurochem. 46, 1444–1451.
Zschaler, J., Schlorke, D., Arnhold, J., 2014. Differences in innate immune response between man and mouse. Crit. Rev. Immunol. 34, 433–454.